SKB

TECHNICAL REPORT 94-26

A surface chemical model of the bentonite-water interface and its implications for modelling the near field chemistry in a repository for spent fuel

Erich Wieland[1], Hans Wanner[1], Yngve Albinsson[2], Paul Wersin[3], Ola Karnland[4]

1 MBT Umwelttechnik AG, Zürich, Switzerland
2 Chalmers University of Technology, Gothenburg, Sweden
3 MBT Technología Ambiental, Cerdanyola, Spain
4 Clay Technology AB, Lund, Sweden

July 1994

SVENSK KÄRNBRÄNSLEHANTERING AB
SWEDISH NUCLEAR FUEL AND WASTE MANAGEMENT CO

BOX 5864 S-102 40 STOCKHOLM
TEL. 08-665 28 00 TELEX 13108 SKB S
TELEFAX 08-661 57 19

A SURFACE CHEMICAL MODEL OF THE BENTONITE-WATER INTERFACE AND ITS IMPLICATIONS FOR MODELLING THE NEAR FIELD CHEMISTRY IN A REPOSITORY FOR SPENT FUEL

Erich Wieland[1], Hans Wanner[1], Yngve Albinsson[2], Paul Wersin[3], Ola Karnland[4]

1 **MBT Umwelttechnik AG, Zürich, Switzerland**
2 **Chalmers University of Technology, Gothenburg, Sweden**
3 **MBT Tecnología Ambiental, Cerdanyola, Spain**
4 **Clay Technology AB, Lund, Sweden**

July 1994

Swedish Nuclear Fuel and Waste Management Co. (SKB)

TECHNICAL REPORT

A surface chemical model of the bentonite-water interface and its implications for modelling the near field chemistry in a repository for spent fuel

Erich Wieland [1]), Hans Wanner [1]), Yngve Albinsson [2]), Paul Wersin [3]) and Ola Karnland [4])

1) MBT Umwelttechnik AG, Zürich, Switzerland
2) Chalmers University of Technology, Gothenburg, Sweden
3) MBT Tecnologia Ambiental, CENT, Cerdanyola, Spain
4) Clay Technology AB, Lund, Sweden

July 1994

MBT Umwelttechnik AG
Vulkanstrasse 110 CH - 8048 Zürich
Environmental

Abstract

Understanding the surface chemical properties of montmorillonite in near-neutral and alkaline media is essential for establishing a chemical model of the bentonite/water interaction applicable for repository conditions. A pretreated and well-characterised Wyoming MX-80 bentonite has been used for investigating the acid/base characteritics of Na-montmorillonite. The CEC of Na-montmorillonite was determined to 108 meq/100 g for pretreated bentonite and to 85 meq/100 g for the bulk material. The BET surface area was (31.53±0.16) m^2/g.

Potentiometric titrations of montmorillonite suspensions at ionic strengths I = 0.005 M, 0.05 M and 0.5 M were conducted as batch-type experiments. Deprotonation of surface OH groups possibly exposed at the edge surface causes an overall negative charge (given by a negative value in the proton balance) on the surface of montmorillonite in the alkaline pH range. In this pH range, the protolysis degree of OH groups increases with increasing pH and ionic strength. The proton density on the surface of montmorillonite increases with decreasing pH in the acidic pH range (pH < 7.5). In this pH range, two simultaneously occurring surface reactions account for the observed proton density on montmorillonite: Protonation of edge OH groups and ion exchange of the major cations for H^+ at the structural-charge sites.

The experimental results are interpreted in terms of a two-site model with structural-charge surface sites (X layer sites) and variable-charge surface sites (edge OH groups) as the reactive surface functionalities. The total population of the surface sites are estimated to TOT-OH = 2.84×10^{-5} mol/g, TOT-X = 2.2×10^{-5} mol/g. The intrinsic acidity constants for the OH groups are determined to pK_{a1}^{int} = (5.4 ± 0.1) and pK_{a2}^{int} = (6.7 ± 0.1), respectively, using the configuration of the diffuse double layer model (DDLM). The thermodynamic constant for the Na/H exchange at structural-charge sites is estimated to $\log K_X^\circ$ = (4.6 ± 0.2).

Experimental data of the potentiometric titration of montmorillonite which are reported in the open literature can be interpreted within the scope of the presented two-site model for montmorillonite by implementing a third type of surface sites, denoted as Y layer sites. The characteristic parameters for the second type of layer sites (Y layer sites) are: TOT-Y = 1.06×10^{-3} mol/g for pretreated Wyoming MX-80 bentonite and 8.3×10^{-4} mol/g for raw Wyoming MX-80 bentonite, respectively, and $\log K_X^\circ$ = 3.0.

Ca-Na-exchange isotherms were measured on pretreated Wyoming MX-80 bentonite. The thermodynamic exchange constant was estimated to $\log K_X^\circ$ = (0.43 ± 0.17).

The near field chemistry under repository conditions is predicted based on the proposed three-site bentonite model. Model computations indicate that the edge OH groups of montmorillonite excert a strong control on the buffer capacity in highly compacted bentonite. Model calculations predict a pH value of 7.3 and and an alkalinity of 1.92×10^{-2} eq/dm^3 in the porewater of highly compacted bentonite.

Long-term predictions of the near field chemistry are presented on the basis of the mixing tank model. The evolution of the chemical composition of bentonite porewater and the relative proportion of exchangeable cations on montmorillonite are established for Allard and Äspö groundwaters in contact with compacted bentonite. The model suggests that pH and alkalinity of the porewater are controlled by the buffering capacity of the edge surface sites and calcite dissolution. In contact with Allard groundwater, the pH values of the porewater in compacted bentonite range from pH = 7.1 - 8.4 depending on the stage of conversion of Na-bentonite to Ca-bentonite. The corresponding pH range for Äspö groundwater is pH = 6.0 - 6.5. The transformation of Na-bentonite to Ca-bentonite strongly depends on the amount of calcite present in bentonite and the chemical composition of the groundwater. Once the carbonate pool is depleted, the conversion of Na-bentonite to Ca-bentonite proceeds at a much lower rate.

Abstract (Swedish)

Förståelse för de ytkemiska egenskaperna hos montmorillonite i neutrala och alkalina media är nödvändigt vid utvecklingen av en kemisk modell för bentonit/vatten interaktioner för tillämpningar vid förvarsförhållanden. En förbehandlad och välkaraktäriserad Wyoming MX-80 bentonit har använts för undersökning av syra/bas egenskaper hos en Na-montmorillonit. CEC hos Na-montmorillonit bestämdes till 108 meq/100 g hos förbehandlad bentonit och 85 meq/100 g hos bulk materialet. BET arean var (31.53±0.16) m^2/g.

Montmorillonitlösningar med jonstyrkorna I = 0.005 M, 0.05 M och 0.5 M titrerades potentiometriskt i batch experiment. Deprotoneringen av yt OH-grupper vid kant ytan skapar en negativ laddning (negativt värde i proton balansen) på montmorillonitens yta i det alkalina pH-området. Protolysgraden av OH-grupperna ökar med ökande pH och jonstyrka i detta pH-område. Proton tätheten på montmorillonit ytan ökar med sjunkande pH i det sura pH-området (pH > 7.5). I detta område är det två samtidiga ytreaktioner som påverkar den observerade protontätheten på montmorilloniten: Protonering av kant OH-grupper och jonbyte mellan katjoner och H^+ på strukturladdningspositionerna.

Experiment resultaten tolkas som en två-positions modell med strukturladdnings ytpositioner (X layer sites) och variabel-laddnings kantpositioner (edge OH groups) som de reaktiva ytfunktionerna. Den totala förekomsten av ytpositioner uppskattas till TOT-OH=$2.84\cdot10^{-5}$ mol/g, TOT-X=$2.2\cdot10^{-5}$ mol/g. Den reella syrakonstanten för OH grupperna är bestämd till pK_{a1}^{int} = (5.4±0.1) och pK_{a2}^{int} = (6.7±0.1) om konfigurationen från "the diffuse double layer model" (DDLM) används. Den termodynamiska konstanten för Na/H jonbyte vid strukturladdningspositionerna bedöms till log K_x° = (4.6±0.2).

Experimentella data, rapporterade i den öppna litteraturen, av potentiometrisk titrering av montmorillonit kan tolkas inom den presenterade två-positionsmodellen genom att införa en tredje typ av ytpositioner, benämnd "Y-layer sites". De karaktäristiska parametrarna för denna andra typ av ytpositioner är: TOT-Y=$1.06\cdot10^{-3}$ mol/g för förbehadlad MX-80 och $8.3\cdot10^{-4}$ mol/g för råmaterialet och log K_x° = 3.0.

Ca-Na-jonbytesisotermer har mätts på förbehadlad MX-80 bentonit. Den termodynamiska utbyteskonstanten bedömdes till log K_x° = (0.43±0.17).

Närområdeskemin under förvarsförhållanden är predikterad med den föreslagna tre-positionsmodellen för bentonit. Modellberäkningarna indikerar att kant OH-grupperna har stor betydelse för buffert kapaciteten i högkompakterad bentonit. Beräkningarna predikterar ett pH på 7.3 och en alkalinitet på $1.92\cdot10^{-2}$ eq/dm^3 i porvattnet i högkompaterad bentonit.

Långtids prediktionerna av närområdeskemin är baserade på en tankreaktor modell. Förändringarna med tiden av den kemiska sammansättningen av bentonitporvattnet och den relativa fördelningen av jonbytare katjoner på montmorilloniten har beräknats för Allard och Äspö grundvatten i kontakt med kompaterad bentonit. Modellen antyder att porvattnets pH och alkalinitet bestäms av bufferkapaciteten hos kantpositionerna och kalcitupplösning. pH-

värdet på porvattnet i högkompakterad bentonit ligger mellan 7.1-8.4 i kontakt med Allardvatten, beroende på graden av omvandling mellan Na-bentonit och Ca-bentonit. För Äspövatten är motsvarande område 6.0-6.5. Omvandlingen från Na-bentonit till Ca-bentonit beror i huvudsak på mängden kalcit i bentoniten samt grundvattensammansättningen. När karbonatförrådet är uttömt går omvandlingen mycket långsammare.

Table of Contents

1 Introduction

Bentonite clay is envisaged as buffer material in a repository for spent nuclear fuel. The interaction of deep groundwaters with the clay material strongly affects the migration of radionuclides. In particular, surface reactions at the clay/water interface, such as ion exchange and protonation and deprotonation reactions, exert control over both pore water and clay composition.

Modelling of the bentonite-water interactions over time requires information on the surface properties of the clay fraction which consists of montmorillonite. It has been suggested in a recent report (Wanner et al., 1992) that the transformation of Na-bentonite to Ca-bentonite over time may be affected by the reactivity of edge sites on the clay as illustrated by Figure 1.

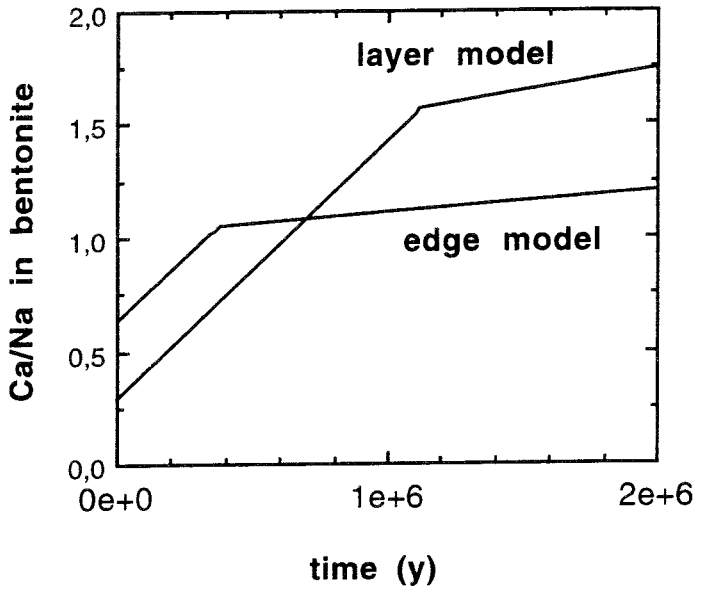

Figure 1 Estimation of the variation of the Ca/Na ratio in highly compacted bentonite over time (years) according to the mixing tank model assuming a time of 13'800 years for one water exchange cycle. From Wanner et al. (1992).

The experimental data on the surface properties under alkaline conditions, i.e., conditions expected in a repository, is extremely scarce (e.g., Marshall and Krinbill, 1942; Avena et al., 1990). This induced us to propose an experimental programme focussing on the determination of the surface-chemical parameters for montmorillonite which are a prerequisite to adequate geochemical modelling of the bentonite system over time.

In this report, we will present the result of an extended experimental approach for the evaluation of the surface chemical parameters for montmorillonite. We first report the pretreatment procedure for raw bentonite. We then summarize and discuss the experimental results of the alkalimetric and acidimetric titration as well as the Ca-Na-exchange isotherms.

2 Material and methods

2.1 Pretreatment and characterisation of bentonite

2.1.1 Preparation of Na-montmorillonite

Na-montmorillonite has been prepared from the commercial bentonite MX-80 available from American Colloid. Characterisation of Wyoming Na-bentonite MX-80 has recently been reported by Kruse (1992). In that study, the mineral composition of raw bentonite was determined to montmorillonite 67.2%, kaolinite 7.1%, illite 3.7%, feldspars 8.8%, quartz 10% and carbonate 2%. According to Kruse (1992), the major part of the accessory minerals was removed by exclusion of the fraction larger than 2 μm. In our study, bentonite has been pretreated using the procedure given by Sposito et al. (1981) in order to remove carbonate impurities. About 500 g of the less than 2 μm fraction was flocculated by adding 8 dm^3 of a solution containing 0.001 M HNO_3 in 1.0 M $NaNO_3$. The flocculated clay was then divided into centrifuge bottles and centrifuged at 4000 r.p.m. for 10 min. The supernatant from each sample was decanted. The pH of the supernatant was measured. The clay was then redispersed in 1.5 times the original volume of the $NaNO_3$-HNO_3 solution and, after shaking for 20 min, again centrifuged. The procedure was repeated until the pH of the supernatant had dropped to pH = 3.0 which was usually achieved after 5 washings (instead of 10 washings as reported by Sposito et al.,1981). The clay was then redispersed in 0.1 M $NaNO_3$ until the pH of the solution had stabilised between pH 5.1 and 5.3. Again these pH conditions were accomplished earlier than reported by Sposito et al. (1981), i.e. after a maximum of 8 washings instead of 10 to 15 washings. The last two cycles were

performed in 0.01 M $NaNO_3$ under argon. The time for centrifuging the samples was extended to 20 min in order to facilitate decanting of the supernatant. The clay was then redispersed in 0.01 M $NaNO_3$ solution and stored in a refrigerator in glass flasks under argon.

2.1.2. Characterisation of the pretreated bentonite

2.1.2.1 XRD

Bentonite material was sampled from the suspension after completing half of the pretreatment and at the end of the pretreatment procedure. Oriented specimens were prepared with the aid of vacuum settling of the suspension onto a ceramic tile. The specimens were then transferred to glass sample holders and placed with the previous downward side upwards. Since the coarser material was on top of the specimens, reflections from possible accessory materials were enhanced. The recordings were made using a Philips PW 1730 machine equipped with a copper anode (CuKα-radiation). The results were digitised and normalised relative to the reflection intensities of quartz. The analyses were made with special attention to carbonate reflections and reflections of the basal spacings of (00*l*) of the clay. The results of the analyses are summarised in Figures 2 and 3.

The recorded 12.45 Å d-spacing, typical for Na-montmorillonite, indicates that no structural transformation has taken place during the pretreatment of bentonite. Most of the feldspar and quartz particles have been separated from the suspension in the >2 μm fraction. Small amounts of calcite are found in the samples taken after half of the pretreatment procedure has been completed. After completion of the entire pretreatment procedure, no typical peaks indicating the presence of calcite, quartz or cristobalite are observed.

2.1.2.2 The cation exchange capacity (CEC) of Na-montmorillonite

The cation exchange capacity was determined with a modified Chapman ammonium acetate method in order to avoid problems with interfering carbonates. Approximately 1 g of clay from each sample was transferred from the original cation into an ammonium state by repeated washings with 1 M ammonium acetate solutions. The concentrations of extracted cations were determined in the supernatants resulting from the washings. The ammonium saturated clay samples were then washed with propanol in order to remove excess ammonium acetate. Ammonium was then replaced by sodium by repeated washings in 2 M NaCl solution. The supernatants resulting from

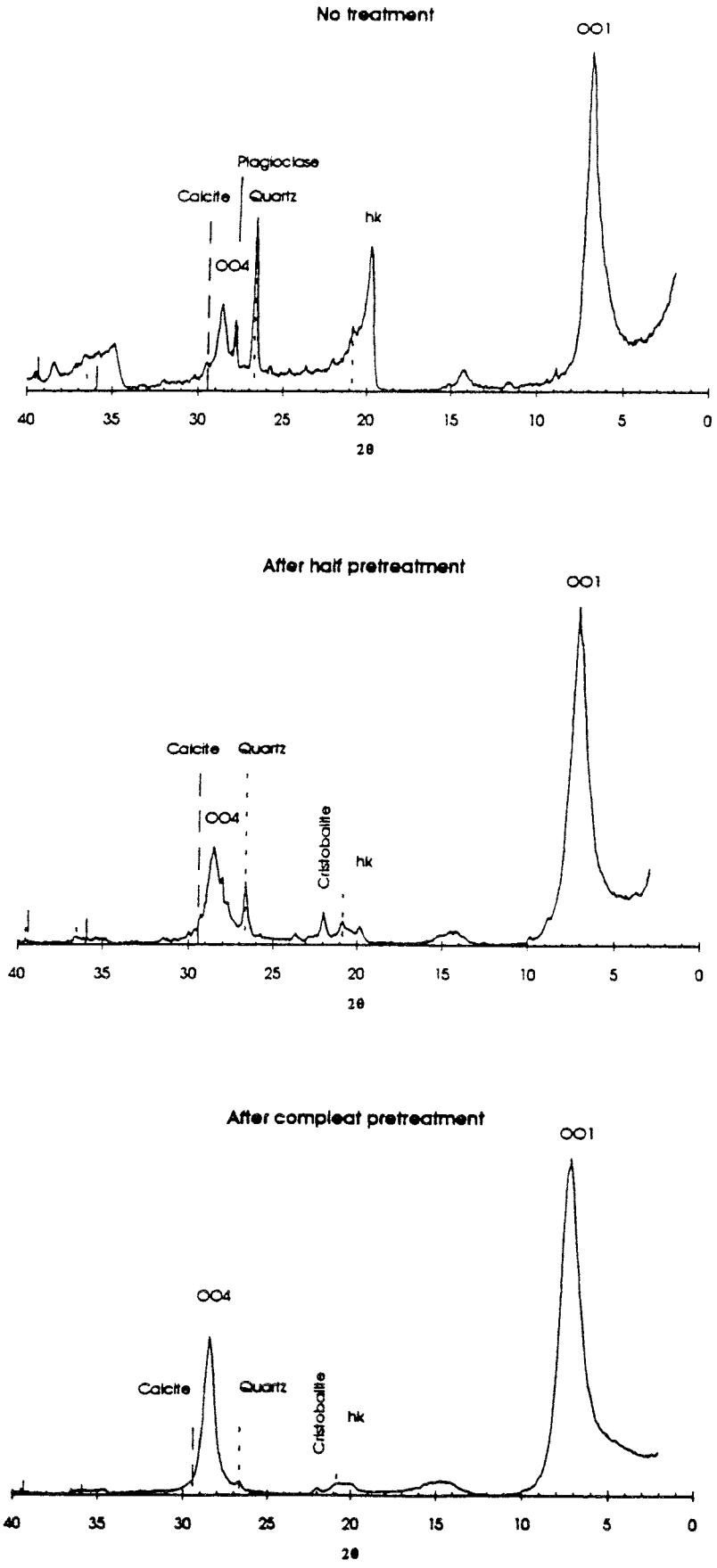

Figure 2 XRD diagrams from the different stages in the treatment.

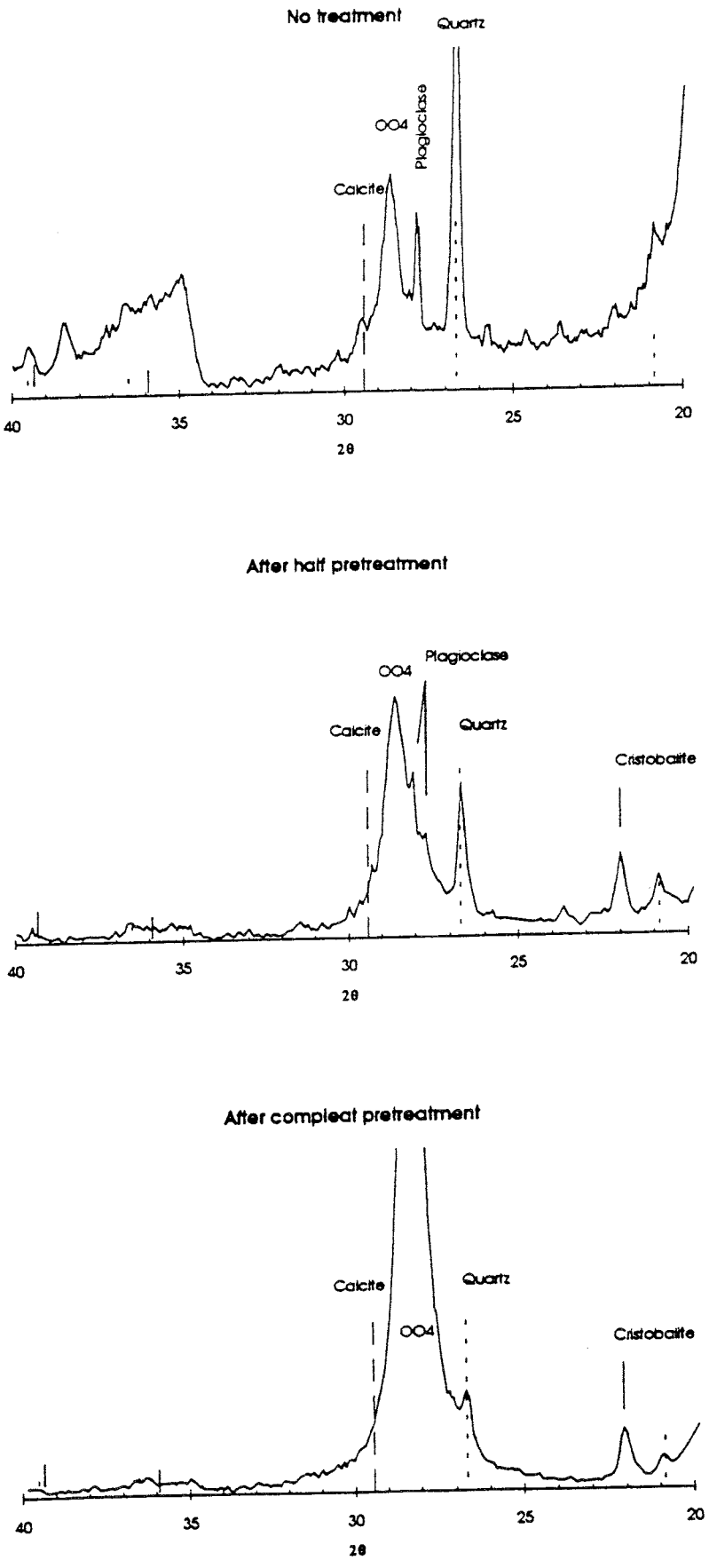

Figure 3 Close up of the XRD diagrams showing the main peaks of calcite.

the washings were analysed for ammonium. Reported CEC values are based on these measurements and not on the concentration of the initially extracted cations. The pH was kept at pH 7 during the procedure using HCl for pH adjustments.

The CEC analyses were made on a bentonite sample after separation of the > 2μm fraction, after the first washings in 0.01 M $NaNO_3$ and finally after completing the entire series of titration experiments. The cation exchange capacity is 81 and 87 meq/100 g for the bulk material, and 108 meq/100g for pretreated Na-montmorillonite, repectively. The sodium contents are 53, 117 and 108 meq/100 g, respectively. The low concentration of sodium in the first analyses is due to the presence of calcium in the original material. The fact that only one washing was made in the 0.01 M $NaNO_3$ solution explains the presence of excess sodium in the second analysis.

For diluted suspensions, the CEC of Na-montmorillonite is assumed to be 108 meq/100 g. In compacted bentonite, the CEC is set to 85 meq/100 g which is in agreement with the CEC value of 72.8 meq/100g for raw bentonite MX-80 reported by Kruse (1992). The value is also consistent with CEC's determined for Wyoming bentonites, i.e., 74 - 95.2 meq/100g (Zysset 1992).

2.1.2.3 The BET surface area

The BET surface area of the pretreated bentonite is determined to (31.53±0.16) m^2/g. Kruse (1992) measured a BET surface area of 35 m^2/g for raw bentonite. The BET surface area accounts for the surface area of the outer basal planes and the edge faces. The specific surface area A_b of the basal plane can be estimated from the dry density ρ [kg/m^3] and the thickness of a silicate layer, z (Zysset, 1992).

$$A_b = \frac{2}{z\rho} \qquad (1)$$

A specific surface area for basal planes of about 740 m^2/g results for a layer thickness of 1 nm and with $\rho = 2.7 \times 10^3$ kg/m^3.

2.1.2.4 Concentration of the stock suspensions

The clay concentration of the montmorillonite suspension was determined by placing 10 ml of the stock suspension in a tarred, acid-washed, 10 ml porcelain crucible. The suspension was dried on a hot plate for 12 hours at low heating, followed by oven drying at 105 °C for 24 hours. After cooling the sample for 3 hours in a vacuum desiccator, the combined weight of dried clay and $NaNO_3$ was measured. The

electrolyte concentration of the stock solution was determined to 0.0095 M $NaNO_3$. The combined weight was corrected for salt contribution to give a net weight of 11.25 g/dm^3 bentonite in the stock suspension.

A second stock suspension was prepared with the following characteristics: 11.80 g/dm^3, I = 0.0185 M.

2.2 *Potentiometric Titrations*

The aim of the potentiometric titration of montmorillonite suspensions was to evaluate the interaction of protons and hydroxyl ions with the clay mineral surface. The experimental procedure requires exclusion of CO_2 from the system, calibration of the electrode in an ionic medium of the same concentration and composition as used in the subsequent titration experiments, and analyses of the solutes which are likely to interfere with surface reactions.

2.2.1 *Apparatus*

Calibration of the pH electrode was performed in a air-tight, well-stirred reaction vessel immersed in a thermostated bath at t = (22±0.1)°C. The pH values were recorded with a glass electrode G202C from Radiometer Copenhagen. A double-junction Hg/Hg_2Cl_2 electrode (K102 from Radiometer Copenhagen) was used as reference electrode. The titrations were performed using a autoburette ABU91 connected to the automatic titrator TIM90 titration manager (all from Radiometer Copenhagen). A VIT90 titrator from Radiometer Copenhagen was used for manual titrations.

2.2.2 *Calibration of the pH electrode*

Prior to potentiometric titrations, an acid/base calibration of the pH electrode was conducted in a medium of the same ionic strength as used in the subsequent titration experiments. With this procedure, pH is calibrated as $-\log[H^+]$ concentration at a given ionic strength. Calibration of the electrode for alkalimetric titrations was done as follows: A well defined, but small (~1.5 ml) volume of 0.1 M HCL was added to 50 ml $NaNO_3$ solution of a given ionic strength (I = 0.005 M, 0.05 M and 0.5 M). After purging the electrolyte solution for 1h with argon (previously passed through CO_2-scrubber), 0.187 M NaOH solution was added in steps of 20 µl up to pH ~11. E.m.f. readings were constant within 2 min after addition of base. For acidimetric titrations

performed in the pH range 3 - 7, 1.5 ml of 0.1 M NaOH were titrated with 0.0225 M or 0.205 M HNO_3.

2.2.3 Titration of montmorillonite suspensions

100 ml bentonite suspension (11.25 g/dm^3 and I = 0.0095 M, or 11.80 g/dm^3 and I = 0.0185 M) were added to 125 ml of a $NaNO_3$ solution. Prior to use, the $NaNO_3$ solution was purged with argon for 1h. The initial concentration of the electrolyte solution was adjusted to give a total concentration of 0.005 M, 0.05 M or 0.5 M $NaNO_3$ in 225 ml clay suspension. The pH of the freshly mixed suspension was constant within 30 min and ranged from 6 to 7.5 depending on the electrolyte concentration. Alkalimetric titrations were performed in the pH range 7 to 11.5. Small volumes of 20 µl to 40 µl of a 0.0177 M NaOH solution were added to the clay suspension. After a total volume of 0.5 ml weak base had been added, the suspension was titrated with 0.187 M NaOH up to a final pH ~10.7. Acidimetric titrations were conducted in the pH range 3 to 7. Small volumes of 20 µl to 40 µl of a 0.0177 M HNO_3 solution were added to the clay suspension. E.m.f. readings were recorded after 1 min, 5 min and 10 min after addition of the titrant. Drifts in the measured potential were between 0.5 and 1 mV in most cases, but in all cases less than 2 mV, between the readings after 5 and 10 minutes.

2.3 Na^+ - Ca^{2+} exchange

10 ml of the stock suspension were equilibrated with solutions of varying Ca/Na ratios. The samples were then reacted for 7 days on a shaker. After centrifuging the samples the pH of the supernatant was measured. Na and Ca were analysed in the supernatant after extraction from the solid with the aid of ion chromatography.

2.4 Chemicals

HCl and NaOH titrants used in the potentiometric titration experiments were prepared as follows: 0.1 M HCl was prepared from Merck titrisol. NaOH solutions were prepared by dissolving NaOH pellets in CO_2-free water. NaOH titrants were calibrated with HCl prior to titrations (0.0177 M and 0.187 M). Electrolyte solutions (e.g., $NaNO_3$ and $CaNO_3$) were prepared from analytical reagent grade chemicals (Merck, p.a.) and bidistilled water.

3 Experimental results

3.1 Potentiometric titrations

3.1.1 Gran calibration of the electrode system

The cell potential, E, of the pH electrode is expressed as a function of the proton concentration $\log[H^+]$ in a solution of a given ionic strength by

$$E = E_0 + s \log[H^+] \qquad (2)$$

The slope, s, and E_0 of the electrode are determined from a linear regression through the data points in the acid range of the calibration curve. The calibration parameters s and E_0 are listed in Table 1. The equivalence volume, V_E, and the ion product of water, K_W, are determined by plotting the experimental data in terms of a Gran function.

The proton balance in the acidic pH range is given by

$$[H^+] = \frac{H_0 V_0 - v\, c_b}{V_0 + v} \qquad [M] \qquad (3)$$

where H_0 is the initial acidity [mol/dm^3], V_0 denotes the initial volume [dm^3], c_b and v represent the concentration [M] and volume [dm^3] of a strong base added to solution.

Gran's graphical method requires linearization of Eq. (3)

$$F_1 = 10^{-pH}(V_0 + v) = c_b(V_E - v) \qquad (4)$$

with V_E as the equivalence volume of strong base added to neutralise the initial acidity. In this context pH represents $-\log[H^+]$. In a Gran plot the function $F_1 = 10^{-pH}(V_0 + v)$ is plotted versus the volume, v, of added base. The equivalence volume, V_E, corresponds to the volume of strong base added to reach the equivalence point. V_E is determined by extrapolating Eq. (4) to $F_1 = 0$ and dividing the intercept by c_b. Within the experimental error, the expected and experimentally determined the V_E values agree for all calibrations (Table 1).

The equivalence volume, V_E, and the ion product, K_W, are then evaluated from experimental data recorded in the alkaline pH range. At pH > 7, the $[OH^-]$ concentration increases according to:

$$[OH^-] = \frac{vc_b - V_E c_b}{V_0 + v} \quad [M] \quad (5)$$

with

$$[OH^-] = K_W / [H^+] \quad [M] \quad (6)$$

Calculation of the Gran function F_2 requires linearisation of Eq. (5):

$$F_2 = 10^{pH}(V_0 + v) = c_b(v - V_E)\frac{1}{K_W} \quad (7)$$

The Gran function F_2 is plotted as a function of the volume, v, of added base. The equivalence volume, V_E, is determined by extrapolating Eq. (7) to $F_2 = 0$ and dividing the intercept by the slope of the regression curve.

The ion product of water is given by combing Eqs. (2), (5) and (6):

$$K_W = 10^{\left(\frac{E-E_0}{s}\right)}\left(\frac{v\,c_b - V_E\,c_b}{V_0 + v}\right) \quad (8)$$

K_W calculated with Eq. (8) is listed in Table 1 as pK_W. The calibration parameters s and E_0 are derived as mentioned above.

Experimental data of the potentiometric titrations (E and $\log[H^+]$), calibration parameters of the pH electrode (E_0 and s) and calculations related to Gran's method of data evaluation (F_1 and F_2, V_E , K_W) are given in the previous progress report (Wanner et al., 1993).

Table 1: Calibration parameters s and E_0. The equivalence volume, V_E, denote: V_E(calc): theoretical volume of added acid or base at the equivalence point, V_E(exp) at pH < 7: equivalence volume determined in a Gran plot for experimental datas at pH < 7, and V_E(exp) at pH > 7: equivalence volume determined in a Gran plot for experimental datas at pH > 7. Uncertainties represent statistical standard deviations for a 95% confidence level.

Experiment	E_0 [mV]	s	V_E(calc) [ml]	V_E(exp) pH < 7 [ml]	V_E(exp) pH > 7 [ml]	pK_W
Theoretical (t = 22°C)		58.492				-13.88 (I=0.005 M) -13.73 (I=0.05 M) -13.59 (I=0.5 M)
E1-4 (I=0.05 M)	322.50±0.38	58.21±0.11	0.5368	0.5351	0.5335	-13.887±0.044
E2-1 (I=0.05 M)	309.51±0.84	58.94±0.34	0.7321	0.7307	0.7399	-13.810±0.009
E2-2 (I=0.05 M)	311.40±0.68	60.20±0.27	0.7344	0.7349	0.7412	-13.642±0.029
E2-3 (I=0.005 M)	311.45±1.14	61.62±0.47	0.7343	0.7364	0.7433	-13.560±0.009
E2-4 (I=0.005 M)	324.92±3.31	66.89±1.05	0.7364	0.7319	0.7501	-12.942±0.016
E2-5 (I=0.5 M)	313.30±0.73	58.67±0.29	0.7353	0.7350	0.7374	-13.680±0.012
E2-6 (I=0.5 M)	311.58±0.37	58.43±0.15	0.7332	0.7332	0.7385	-13.713±0.013
E2-7 (I=0.005 M)	292.83±1.26	59.34±0.36	0.7450	0.7557	0.7354	-13.923±0.014
E3-3 (I=0.5 M)	330.59±0.74	58.26±0.26	0.8546	0.8552	0.8322	-13.754±0.018
E3-4 (I=0.5 M)	327.81±0.55	58.89±0.18	0.5358	0.5345	0.5340	-13.676±0.016
E3-5 (I=0.5 M)	323.39±0.90	58.45±0.27	0.8160	0.8087	0.8195	-13.696±0.007
E4-3 (I=0.005 M)	324.54±0.87	56.81±0.26	0.8546	0.8533	0.8594	-14.222±0.004
E4-4 (I=0.005 M)	324.27±0.83	59.90±0.26	0.5352	0.5363	0.5331	-13.778±0.023

3.1.2 Proton balance calculations

In principle, the concentration of H^+ and OH^- bound onto the surface of montmorillonite (i.e., the portion of surface charge due to H^+ and OH^- surface interaction in the case of simple oxides) can be calculated from the difference between the total H^+ or OH^- added to the suspension and the equilibrium H^+ and OH^- concentration as a function of pH. The concentration of protons or hydroxyl ions (further denoted $\Delta[H^+]$) bound onto the surface is given by:

$$\Delta [H^+] = \left(\frac{c_A - c_B - [H^+] + [OH^-] - C}{a} \right) \qquad [mol/g] \qquad (9a)$$

or

$$\Delta [H^+] = \left(\frac{[H^+]_t - [H^+] + \frac{K_W}{[H^+]} - C}{a} \right) \qquad [mol/g] \qquad (9b)$$

$[H^+]_t$: $(=c_A - c_B)$ total proton concentration [mol/dm^3]
$[H^+]$: free proton concentration in solution
K_W : ion product of water
C : correction factor for proton consuming side reactions
a : initial suspension concentration [g/dm^3]
$c_A - c_B$: concentrations of added base or acid [mol/dm^3]

$\Delta[H^+]$ is the surface proton (hydroxyl) concentration, c_A and c_B are the total concentrations of added acid and base [mol/dm^3], respectively. The suspension concentration, C_S [g/dm^3], is given by:

$$C_s = \frac{V_0\, a}{V_0 + v} \qquad [g/dm^3] \qquad (10)$$

Since the added volume of acid or base is small compared to the initial volume, V_0, of the suspension ($V_0 >> v$), dilution is negligible during the titration experiments and, hence, $C_S \approx a$.

C denotes a correction factor accounting for proton consumption due to dissolution processes and titration of soluble Al and Si species present in suspension. Parallel titration experiments were run in order to determine the total concentrations of Al and Si in suspensions. Both Si and Al were determined using photometric standard methods (e.g., for Si see Standard methods for examinations of water and wastewater, American Public Health Association, 17th Ed., 1989; for Al see Swedish standard SS 028210, SIS The Swedish Standardisation Commission). Measurements of Al and Si concentrations are summarised in a previous progress report (Wanner et al., 1993).

The correction factor, C, in the proton balance as given in Eqs. (9a) and (9b) accounts for proton consumption due to hydrolysis of Al over the entire pH range and due to deprotonation of monomeric $Si(OH)_4$ in the alkaline pH range. In the acid pH range, contributions of soluble, monomeric hydrolysis products of Al (= $Al(OH)_m^{3-m}$) are considered according to

$$C = \sum_{m=0}^{3} (3-m)\, \beta_{1,m}\, \alpha_H\, [Al]_t\, [H^+]^{-m} \qquad [M] \qquad (11a)$$

with $\alpha_H = (1 + \beta_{1,1}\,[H^+]^{-1} + \beta_{1,2}\,[H^+]^{-2} + \beta_{1,3}\,[H^+]^{-3} + \beta_{1,4}[H^+]^{-4})^{-1}$ and $[Al]_t$ as the total concentration of Al in solution. In the alkaline pH range, the formation of $Al(OH)_4^-$ and the deprotonation of silicic acid, $Si(OH)_4$, are considered as the interfering reactions:

$$C = \beta_{1,4}\, \alpha_H\, [Al]_t\, [H^+]^{-4} + K_1\, [Si]_t\, [H^+]^{-1} \qquad [M] \qquad (11b)$$

with $[Si]_t$ as the total concentration of Si in solution. Equilibrium constants, $\beta_{1,m}$, for Al hydrolysis and the acidity constant, K_1, for silicic acid are taken from Baes and Mesmer (1976).

Deprotonation of $Si(OH)_4$ is the main contribution to corrections in the proton balance. Hence proton balance in the acidic pH range is adequately described by neglecting the correction factor, C, in Eqs. (9a) and (9b). During the titration experiments, the concentration of Si in suspensions ranged between 5×10^{-5} M to 1.2×10^{-4} M. No pH-dependent increase in the Si concentration could be observed over the entire pH range providing further evidence that dissolution of montmorillonite is insignificant under the given conditions. An average Si concentration of 10^{-4} M is assumed for calculating the correction factor. The photometric method used for analysing Si in this study determines Si in the monomeric form $Si(OH)_4$. We hence may assume that during the

titration of montmorillonite suspensions in the alkaline pH range, Si is deprotonated according to the corresponding acid/base equilibrium of monomeric $Si(OH)_4$.

3.1.3 Error estimations for $\Delta[H^+]$

Uncertainties in $\Delta[H^+]$ are estimated from Eq. (9b) as follows: The main contribution to the error in $\Delta[H^+]$ is due to small potential drifts during pH determination. Errors in the concentration of added acid or base are comparatively small, and those in the correction factor C are assumed to be negligible. For the acidimetric titrations, the error in $\Delta[H^+]$ is hence determined by the error in $[H^+]$. For the alkalimetric titrations, the error in $[OH^-]$ accounts for the error in $\Delta[H^+]$. The error in $\log[H^+]$ is estimated from Eq. (2) to:

$$(\sigma_{\log[H^+]})^2 \approx (\sigma_E/s)^2 + (\sigma_{Eo}/s)^2 \qquad (12)$$

The errors in $\log[OH^-]$ can be estimated from Eq. (6):

$$(\sigma_{\log[OH^-]})^2 = (\sigma_{\log Kw})^2 + (\sigma_{\log[H^+]})^2 \qquad (13)$$

With s = 58.56 mV (theoretical slope at t = 22°C), σ_E = 0.5 mV (potential drift during measurements) and σ_{Eo} = 2 mV (error in calibration of the pH electrode), $\sigma_{\log[H^+]}$ is estimated to 0.03 log units. The error in the ion product, $\sigma_{\log Kw}$, results from the evaluation of K_W as given in Table 1. The experimental errors imposed on $\Delta[H^+]$ are smaller than 5 percent for the acidimetric titrations, and hence not specifically indicated in the data plots. However, the propagation of errors leads to significant uncertainties at pH values above 10.

3.1.4 Discussion

Alkalimetric titrations of montmorillonite were performed in the pH range 7 - 11.5. Acidimetric titrations in the pH range 7 - 3.5 were conducted in separate experiments. Ionic strengths of the background electrolyte were I = 0.005 M, 0.05 M and 0.5 M. The concentration of surface protons $\Delta[H^+]$ is calculated for each data point of an experimental run. Proton balance calculations are based on pH measurements recorded after an equilibration time of 10 min. Note that, in this context, pH refers to $-\log[H^+]$ measured at a given ionic strength. Calculations and experimental results are reported in detail in a previous progress report (Wanner et al., 1993).

A summary of all experimental results is given Figure 4. The data base for each concentration of the electrolyte background, i.e., I = 0.005 M, I = 0.05 M and I = 0.5 M,

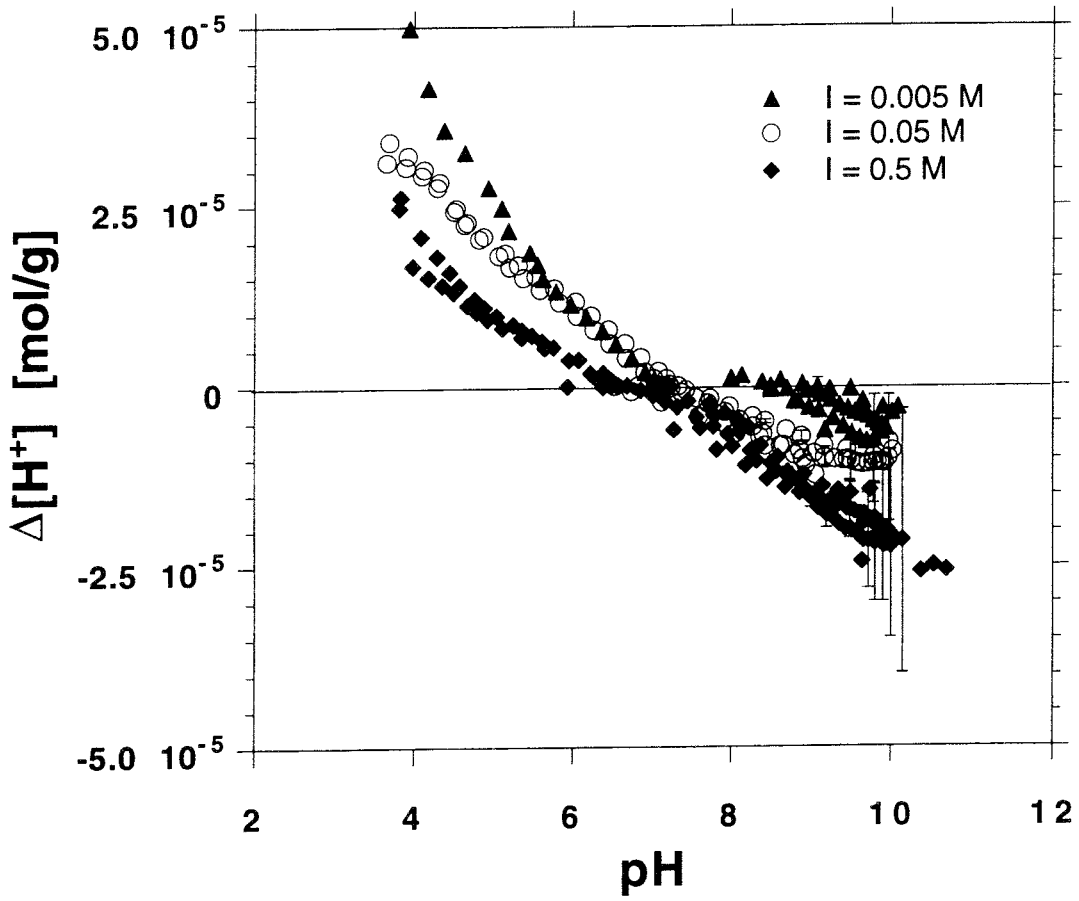

Figure 4 *Titration curves of montmorillonite (5 g/dm^3) at 22°C. The surface proton concentration, $\Delta[H^+]$, is plotted as a function of pH for three different ionic strengths (I = 0.005 M, I = 0.05 M, I = 0.5 M).*

includes the results from several experimental runs. Figure 4 hence shows that the titrations of montmorillonite suspensions are reproducible for all concentrations of the electrolyte background. Figure 4 further reveals that two distinct branches of the titration curve exist: $\Delta[H^+]$ is negative in the alkaline pH range representing deprotonation of the montmorillonite surface, and positive in the acidic pH range due to protonation of surface functional groups. The degree of deprotonation increases with increasing ionic strength in the alkaline pH range. This characteristic behaviour of mineral surfaces is typically observed in the case of simple oxides such as γ-Al_2O_3,

TiO_2 or FeOOH (cf. Figure 6 and James and Parks, 1982). It indicates that deprotonation of surface OH groups causes the negative charge (i.e., $\Delta[H^+] < 0$) on the surface of montmorillonite. Hence, the results presented in Figure 4 provide convincing evidence for the fact that the acid/base properties of montmorillonite in the alkaline pH range are due to ionisation of OH groups existing at the surface. From structural arguments we may infer that the reactive OH groups are likely exposed at the edge face of a montmorillonite platelet.

There is no unique PZSE (point of zero salt effect) for montmorillonite suspensions (Figure 4). The PZSE is the pH value at which titration curves obtained at different ionic strengths of the background electrolyte solution meet. Whereas the PZSE of oxides is well defined, a unique PZSE has not been found in suspensions of 2:1 phyllosilicates (Gallez et al., 1976; Madrid et al., 1983, 1984; Madrid and Diaz-Barrientos, 1988; Avena et al., 1990). Figure 4 reveals that conditions where $\Delta[H^+] = 0$ are met in the pH range 6.5 - 8 depending on the concentration of the background electrolyte. The PZNPC (point of zero net proton conditions) denotes the pH value where $\Delta[H^+] = 0$. Below the PZNPC of montmorillonite, the concentration of proton adsorbed on the surface, $\Delta[H^+]$, increases with decreasing pH. However, the sequence in the ionic strength dependence of the titration curves is in conflict with experimental observations made for oxides. Figure 4 shows that the concentration of protons adsorbed on the surface, $\Delta[H^+]$, decreases with increasing ionic strength. If OH groups were the only surface functional groups accounting for the acid/base properties of montmorillonite in the acidic pH range, an increase in $\Delta[H^+]$ with increasing ionic strength would be expected. Such a dependence of surface proton concentration upon ionic strength has been reported for simple oxides such as γ-Al_2O_3 (James and Parks, 1982). We hence may conclude that the OH groups of the edge face which account for experimental observations in the alkaline pH range are not the only surface functional groups reacting with protons in the acidic pH range. The reversal of the ionic strength dependence of $\Delta[H^+]$ in the acidic pH range can only be explained if we assume that protons react with a second type of surface sites in an ion-exchange type of reaction. The second type of surface functional groups on montmorillonite reacting with protons are structural-charge surface sites (Anderson and Sposito, 1991). Structural-charge surface sites carry a permanently negative charge due to isomorphic substitutions in the tetrahedral and octahedral layers. This type of sites, in the following denoted as X layer sites, gives rise to the cation exchange capacity observed in clay minerals. Their chemical reactivity is mainly due to ion exchange reactions occurring at these sites.

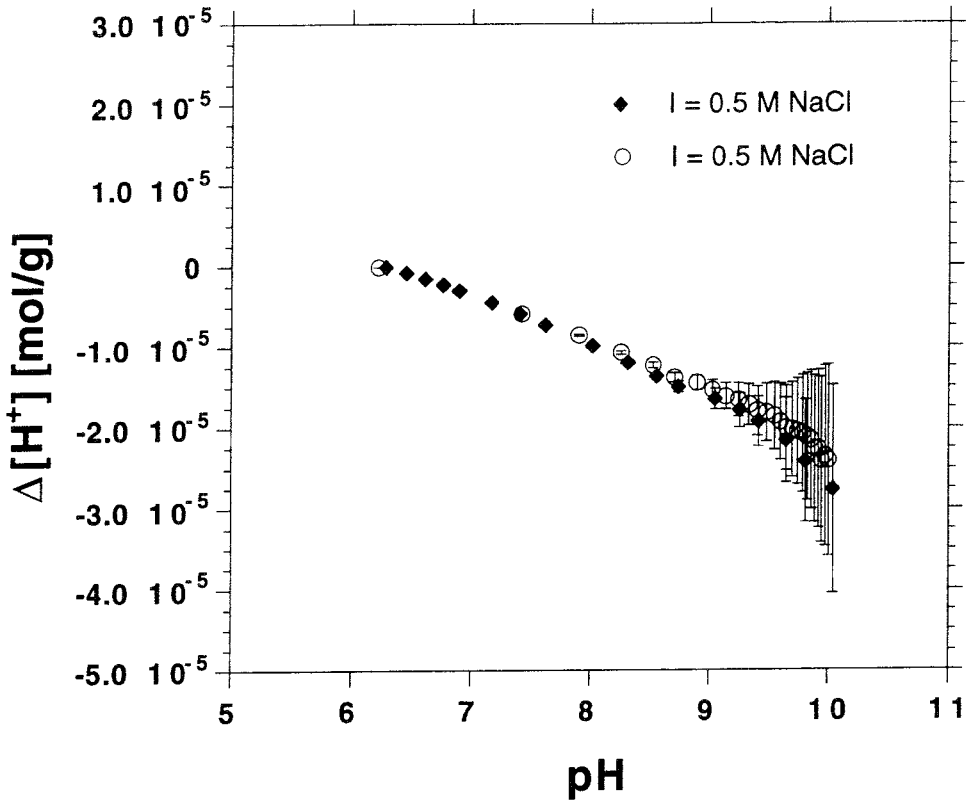

Figure 5 *Titration curves of montmorillonite as a function of pH (montmorillonite 5 g/dm^3, I = 0.5 M NaCl). The error bars reflect the propagation of errors when a constant uncertainty in pH is assumed.*

The experimental data of two titrations conducted in 0.5 M NaCl are displayed in Figure 5. The experimental data obtained in 0.5 M $NaNO_3$ (Figure 4) and in 0.5 M NaCl (Figure 5) overlap (not shown) which can be interpreted as evidence for the absence of specific interactions of Cl^- with ionisable surface OH groups.

3.2 Na^+ - Ca^{2+} exchange

3.2.1 Presentation of the experimental data

Na/Ca adsorption is studied by reacting montmorillonite with solutions of varying but known Na/Ca compositions. The chemical analysis is carried out after centrifugal

separation of the solid from the supernatant. This kind of separation requires a concentration correction for the reactant solution entrained with the clay. The moles of chemical species i adsorbed per kilogram of dry clay contacting an aqueous solution is calculated with (Sposito, 1981):

$$q_i = n_i - M_w m_i \qquad \text{[mol/kg]} \qquad (14)$$

where n_i is the total moles of species, i, per kilogram of slurry (dry clay minus entrained solution slurry); M_w is the gravimetric water content of the slurry (kg water per kg dry clay); and m_i is the molality (or molarity) (moles per kg water) of species, i, in the supernatant solution. Eq. (14) represents the surface excess, q_i, of a chemical species. If the surface excess of Ca and Na and their equilibrium concentration in solution is determined, an exchange isotherm can be constructed. An exchange isotherm is analogous to an adsorption isotherm except that the variables plotted are charge fractions instead of surface excesses and concentrations (Sposito, 1981). The equivalent fraction, E_i, of the adsorbed cation is:

$$E_i(\text{clay}) = |Z_i| q_i/Q \qquad (15)$$

where Z_i is the valence of the cation i, q_i is its surface excess as given in Eq. (14), and Q represents the cation exchange capacity (= 108 meq/100 g). The equivalent fraction, E_i, of a cation, i, in aqueous solution is given by:

$$E_i(\text{sln}) = \frac{|Z_i| c_i}{\sum_k |Z_k| c_k} \qquad (16)$$

where c_i is the concentration of the exchangeable cation, i, in solution and the sum extending over all cations, k, in solution. An exchange isotherm for a specific cation, i, is defined as a graph of E_i(clay) against E_i(sln) at fixed temparature and pressure.

The exchange isotherms for the Na/Ca exchange on Na-montmorillonite are shown in Figure 6. The evaluation of the results is given in detail in a previous progress report (Wanner et al., 1993). The solid curve in Figure 6 is the thermodynamic nonpreference exchange isotherm for a monovalent - bivalent ion exchange given by the equation:

$$E_{Ca} = 1 - \sqrt{\frac{A(1-E_{Ca}(\text{sln}))^2}{E_{Ca}(\text{sln}) + A(1-E_{Ca}(\text{sln}))^2}} \qquad (17)$$

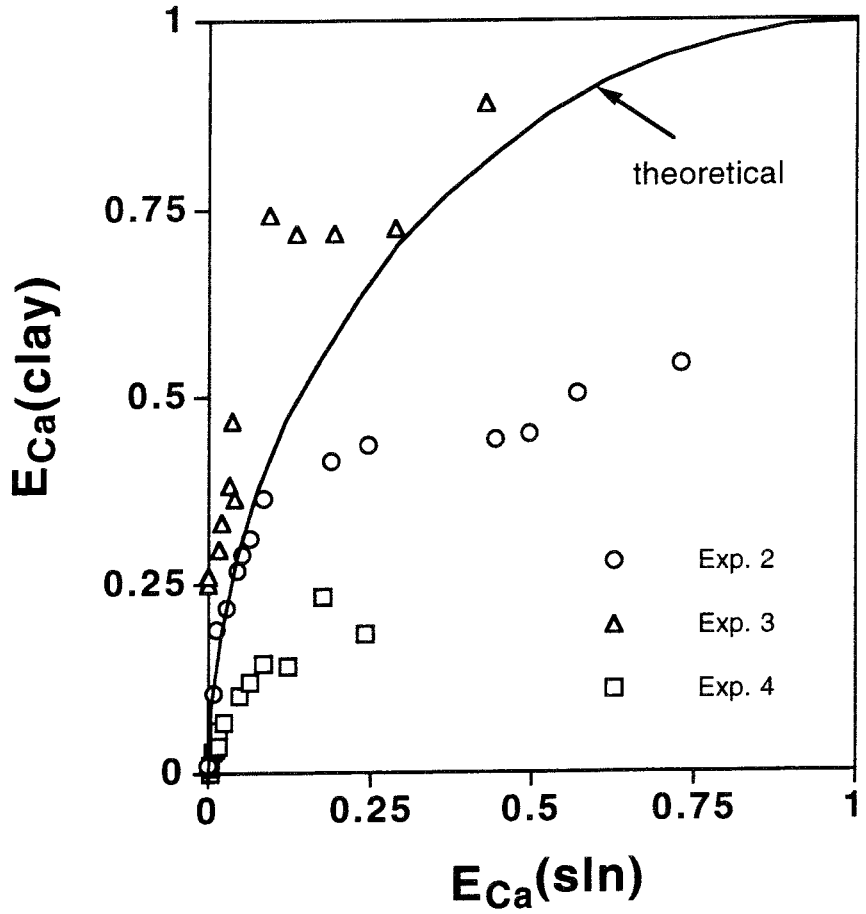

Figure 6 *Exchange isotherm for the Na^+ - Ca^{2+} ion exchange. The experiments were conducted under different conditions: Exp. 2 with 10.06 g/dm^3 montmorillonite at pH ≈ 8, Exp. 3 with 10.06 g/dm^3 at pH ≈ 11 and Exp. 4 with 56 g/dm^3 at pH ≈ 10.*

where E_{Ca}(sln) is the equivalent fraction of Ca and $A = (\Sigma_k Z_k c_k)(\gamma_{Na})^2/2\gamma_{Ca}$. The solid curve is calculated with $\Sigma_k Z_k c_k = 0.046$ mol/dm^3, $(\gamma_{Na})^2/\gamma_{Ca} = 1.45$, so that $A = 0.034$. The nonpreference isotherm describes an ideal ion exchange with a compositional independence of the equilibrium constant. Experimental results above the non-preference isotherm indicate selectivity of montmorillonite for Ca^{2+} relative to Na^+ whereas results below the nonpreference isotherm may be interpreted as selectivity for Na^+.

Sodium-calcium exchange on Wyoming bentonite (i.e., montmorillonite) has been investigated previously by Sposito et al. (1983 a,b). Their results obtained in a montmorillonite suspension with constant 0.05 M perchlorate background and at pH =

7 support a non-preference model for the Na^+ - Ca^{2+} exchange reactions. According to Sposito (1984) and Fletcher and Sposito (1989), montmorillonite reveals an ideal or near-ideal exchange behaviour in the case of Na^+ - Ca^{2+} exchange. Figure 6 shows that in the present study, ideality on montmorillonite is supported in two of the experiments, i.e., in Exp. 3, considering the scatter of the data, and in Exp. 2 at low sorption densities. A significant decline in the preference of montmorillonite for Ca^{2+} is observed in Exp. 2 at high sorption densities (10.06 g/dm^3, pH = 7.5 - 8.5) and in Exp. 4 (59 g/dm^3, pH = 9 - 10.5). Preference and decline of the preference of montmorillonite for a bivalent cation has been observed and attributed to the presence of interfering anions which may affect the affinity of the surface for the exchangable cation (Sposito et al., 1983a).

3.2.2 Thermodynamics of ion exchange reactions

The exchange reaction describing the replacement of Na^+ for Ca^{2+} on Na-montmorillonite is given by:

$$Ca^{2+} + 2\,NaX \Leftrightarrow CaX_2 + Na^+ \qquad K_X^\circ \qquad (18)$$

A value of (1.48±0.3) for the thermodynamic exchange constant, K_X°, has been reported by Fletcher and Sposito (1989). The ion exchange reaction given by Eq. (18) can also be expressed in terms of rational activity coefficients and the Vanselow selectivity coefficient as:

$$K_X^\circ = K_V \frac{(f_{CaX_2})}{(f_{NaX})^2} \qquad (19)$$

with f as the rational activity coefficient of the surface species NaX and CaX_2, and K_V as the Vanselow selectivity coefficient (Vanselow, 1932) given by:

$$K_V = \frac{(x_{CaX_2})(a_{Na})^2}{(x_{NaX})^2(a_{Ca})} \qquad (20)$$

with x_i as the mole fraction of the surface species and a_i as the activities of Na and Ca in solution.

The Vanselow selectivity coefficient is a conditional equilibrium constant which, for non-ideal systems, varies with the composition of the exchanger phase. The cause of

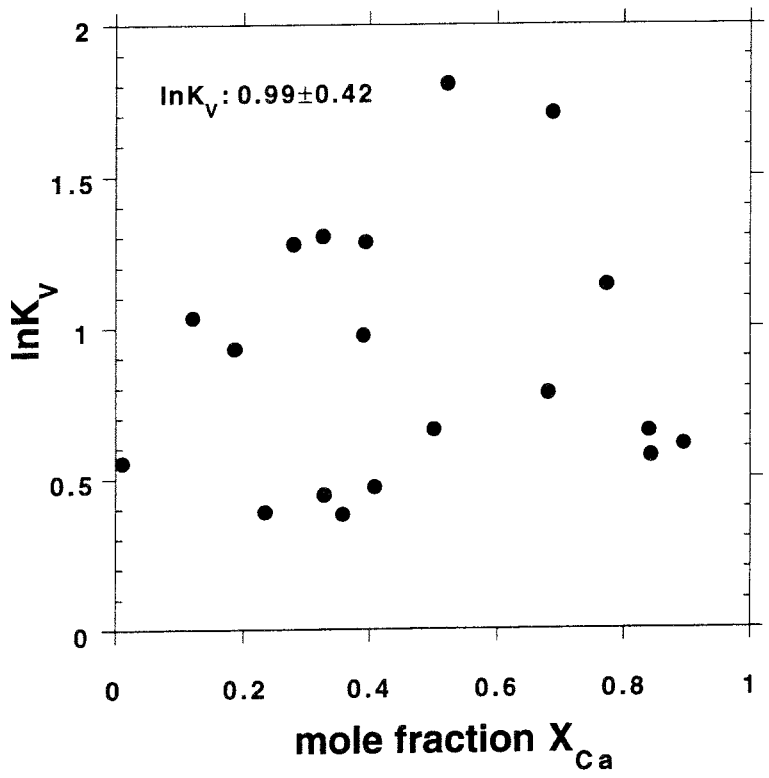

Figure 7 Na^+ - Ca^{2+} exchange on montmorillonite. The Vanselow selectivity coefficient, K_V, is plotted as a function of the mole fraction of CaX_2, x_{Ca}. The mean value for K_V is calculated from the experimental data which follow the theoretical line shown in Figure 6.

the composition dependence of K_V are the interactions between adsorbed species that occur as the adsorbate composition changes. In an ideal solid solution with the rational activity coefficient equal to unity, the thermodynamic constant equals the Vanselow selectivity coefficient as given by Eq. (19). In this case, the Vanselow coefficent, K_V, should be constant for varying equivalent fractions, E_{Ca}(clay), of adsorbed Ca. The Vanselow selectivity coefficient has also been evaluated from the experimental data reported in the present study. Figure 7 shows the exchange constant as a function of the equivalent fraction, E_{Ca}(clay), of adsorbed Ca. Note that the values for K_V which are displayed in Figure 7 are calculated for those conditions where ideality on montmorillonite holds, i.e., Exp. 3 and Exp. 2. The Vanselow selectivity coefficient is determined to (2.63±1.52). However, since the error in the experimental K_V value is rather large, we use K_V values reported in the literature for modelling the Na^+ - Ca^{2+} exchange on montmorillonite

4 A surface chemical model for montmorillonite

Clay minerals contain at least two types of surface functional groups : permanently charged surface functional groups created by ionic substitution within the crystal structure and variably charged surface functional groups caused by ionisation of surface OH groups. The first type of surface sites arises from the isomorphic substitution of Al^{3+} for Si^{4+} within the tetrahedral surface layer causing a permanent charge on the mineral surface. The structural charge is compensated by cations. Hereafter, this type of surface sites is denoted as structural-charge surface sites or simply layer sites.

In addition to the permanent charge of the layer surface, ionisation of surface OH groups which are most likely located at the edge surface of a clay particle also gives rise to a pH-dependent charge. The properties of the surface OH groups of a clay mineral are similar to those found for hydrous oxide surfaces (Stumm and Morgan, 1981; Sposito, 1984; Wieland and Stumm, 1992). The surface OH group on a hydrous oxide reveals chemical properties which are similar to those observed for the corresponding counterparts in dissolved solutes , e.g., hxydroxide ions. Therefore, the strongly pH-dependent charge of OH sites results from protonation and deprotonation reactions as a function of the solution pH. Deprotonated OH groups behave as Lewis bases and form surface complexes with metal ions. Furthermore the adsoprtion of ligands (anions and weak acids) on metal (hydr)oxids can be compared with complex formation reactions in solution. Hereafter, this type of amphoteric surface sites is designated as variable-charge surface sites. Since they are located at the edge face of a montmorillonite platelet, we denote them edge sites.

Note that the variable-charge component of the surface charge, i.e., the surface charge due to hydrolysis reactions of OH groups, is often ignored in investigations of 2:1 layer-type clay minerals. Yet the incorporation of the variable-charge sites in a surface chemical model for 2:1 phyllosilicates is essential to understanding and modelling those surface chemical properties which exhibit a strong pH dependence, such as the apparent CEC, the exchange selectivity, colloidal stability and surface complex formation of metal cations and organic and inorganic anions.

The two-site model for montmorillonite proposed in this study contains two types of surface functional groups which are separate chemical entities with different surface-chemical properties. A better understanding of the surface reactions occurring at structural-charge (layer sites) and variable-charge surface sites (edge sites) is required

in order to adequately model surface-chemical reactions occurring at the surface of montmorillonite.

Modelling the acid/base characteristics of montmorillonite over the entire pH range hence requires the introduction of two types of surface sites: Surface OH groups accounting for the pH-dependent variable-charge sites and structural-charge surface sites which are available for ion exchange reactions. The following abbrevations will be used: SOH for variable-charge surface OH groups and X for the ion exchange sites. Therefore, SOH sites represent edge sites and X sites represent layer sites.

4.1 Surface equilibria at edge and layer sites

4.1.1 Interaction of surface sites with protons and hydroxyl ions

The interaction of protons with layer sites of Na-montmorillonite can be expressed as cation exchange reaction represented by the stoichiometric replacement of H^+ by Na^+:

$$H^+ + NaX \Leftrightarrow HX + Na^+ \qquad K_X^\circ \qquad (21)$$

The thermodynamic equilibrium constant, K_X°, for the Na^+ - Ca^{2+} exchange is given by:

$$K_x^\circ = K_V \frac{(f_{HX})}{(f_{NaX})} \qquad (22a)$$

with the Vanselow selectivity coefficient, K_V, defined by:

$$K_V = \frac{(x_{HX})(a_{Na})}{(x_{NaX})(a_H)} \qquad (22b)$$

In the present study, we consider an experimental system with montmorillonite in its Na-form and $NaNO_3$ as the background electrolyte. As indicated in Eq. (21), the degree of the Na/H replacement on montmorillonite for a given solid/solution ratio then depends on pH and the concentration of the background electrolyte.

The ionisation of OH groups is the characteristic surface reaction occurring at edge sites. Protonation and deprotonation reactions at edge sites are the consequence of the acid base behaviour of surface OH groups:

$$\equiv SOH_2^+ \quad \Leftrightarrow \quad \equiv SOH \quad \Leftrightarrow \quad \equiv SO^-$$

Protonation and deprotonation reactions of edge sites are due to the amphoteric character of the OH groups (cf. e.g., Stumm and Morgan, 1981, Sposito, 1984):

$$\equiv SOH_2^+ \quad \Leftrightarrow \quad \equiv SOH + H^+ \qquad K_{a1}^{app} \qquad (23a)$$

$$\equiv SOH \quad \Leftrightarrow \quad \equiv SO^- + H^+ \qquad K_{a2}^{app} \qquad (23b)$$

where $\equiv SOH_2^+$, $\equiv SOH$ and $\equiv SO^-$ represent positively charged, neutral and negatively charged surface hydroxyl groups of the edge surface, and K_{a1}^{app} and K_{a2}^{app} are apparent acidity constants. The mass law equations corresponding to the reactions given above are:

$$K_{a1}^{app} = \frac{(\equiv SOH)\{H^+\}}{(\equiv SOH_2^+)} \qquad (24a)$$

$$K_{a2}^{app} = \frac{(\equiv SO^-)\{H^+\}}{(\equiv SOH)} \qquad (24b)$$

where ( ) represent concentrations and { } represent activities. The activity coefficients for the surface species are assumed to be equal to unity. K_{a1}^{app} and K_{a2}^{app} are apparent equilibrium constants because they include surface charge effects and, hence, depend on the degree of surface ionisation. For example, with increasing positive surface charge it becomes more difficult to bind protons onto the surface and, conversely, with increasing negative surface charge it becomes more difficult to dissociate protons from the surface.

4.1.2 The diffuse double layer model (DDLM)

A number of different surface complexation models have been proposed in the last two decades. The models are distinguished by differences in their respective molecular hypotheses. Each model assumes a particular interfacial structure resulting in a specific consideration of various kinds of surface reactions and electrostatic correction factors to mass law equations. In the present study, we have chosen an improved version of the diffuse double layer model for a description of the charge-potential relationship of the interfacial region.

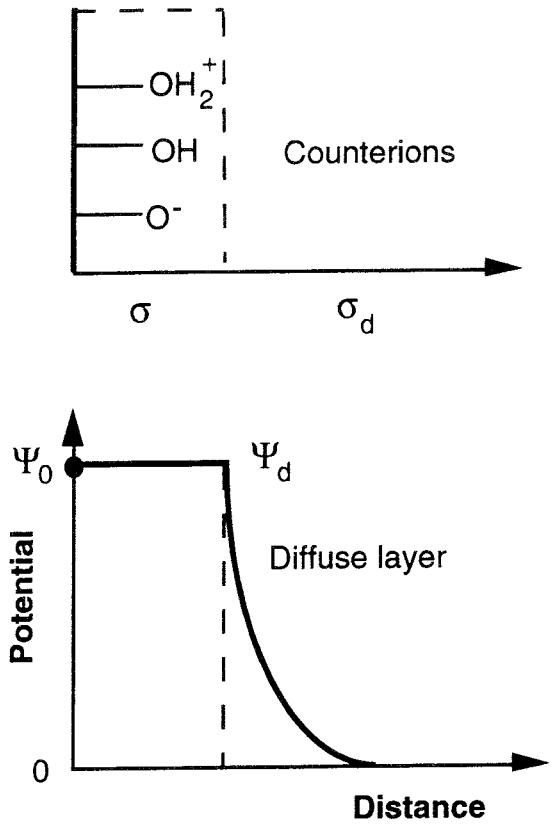

Figure 8 *Schematic representation of ion binding on a mineral surface (upper figure) and the decay of the electrical power with distance from the surface in the diffuse double layer model (lower figure).*

The diffuse double layer model (DDLM) originally proposed by Stumm et al. (1970) and Huang and Stumm (1973) has been reviewed and improved recently by Dzombak and Morel (1990). The principal reasons for chosing the generalized two-layer model as presented by Dzombak and Morel (1990) are: 1) It is the simplest model that has been successfully used to describe qualitatively and quantitatively surface complex formation of protons, cations and anions. 2) The two-layer model has been incorporated in the geochemical speciation code MINEQL (Westall et al., 1976) to give a combined version MIN_SURF (Berner, 1993).

In the DDLM, all ions are adsorbed as coordination complexes within the surface plane, except the dissociated counterions present in the diffuse layer (Figure 8). The charge balance in the electrical double layer is then given by:

$$\sigma + \sigma_d = 0 \tag{25}$$

with σ as the surface charge and σ_d as the counterion charge [C/m^2]. The separation of charges in the electrical double layer results in an electrical difference across the mineral-water interface. The Gouy-Chapman theory describes the distribution of counterions in a diffuse swarm formed at a charged planar surface. In this theory, the distribution of charge and potential within the electrical double layer is given by solutions of the Poisson-Boltzmann equation derived for planar double layer (for a detailed derivation and discussion see Sposito, 1984). The model accounts for the ionic strength effects on ion adsorption through the explicit dependence of the diffuse-layer charge, σ_d, on ionic strength. For a symmetrical electrolyte with valence z, the charge-potential relationship is given by :

$$\sigma_d (= -\sigma) = -0.1174\sqrt{c}\sinh(z\Psi F/2RT) \tag{26a}$$

or at t = 25°C (T = 298.15 K) and z = 1 (Davis and Kent, 1990):

$$\sigma_d (= -\sigma) = 2.5\sqrt{I}\Psi \tag{26b}$$

with z as the valence of the ion, c as the molar concentration of the electrolyte background [M], Ψ as the potential at the surface [V], R as the molar gas constant (= 8.314 J/mol K) and T as the absolute temperature [K]. In the case of an asymmetrical electrolyte, a different charge-potential relationship is involved (Hunter, 1987). The possibility of asymmetrical electrolytes has been accounted for in the MIN_SURF computer code developed by Berner (1993).

The total free energy of sorption of a species onto a surface, e.g., protons as expressed in Eqs. (23a) and (23b), has operationally been separated into a specific, i.e., chemical, and a non-specific, i.e., coulombic, interaction term. The coulombic free-energy term reflects the electrostatic work in transporting ions through the interfacial potential gradient (e.g., Stumm and Morgan, 1981; Morel, 1983). The chemical free-energy term accounts for the energy of interaction of an ion, e.g., protons in Eqs. (23a) and (23b), with surface sites on a hypothetically uncharged surface. The chemical interaction term does not vary with surface charge and, hence, is designated as "intrinsic" free-energy term. A detailed derivation and discussion of the relevant equations are given in, e.g.,

Stumm and Morgan, 1981; Sposito, 1984; Dzombak and Morel, 1990. Applying the concept briefly outlined above, the apparent acidity constants given in Eqs. (24a) and (24b) can be rewritten as:

$$K_{a1}^{app} = K_{a1}^{int}\exp(-F\Psi/RT) \tag{27a}$$

$$K_{a2}^{app} = K_{a2}^{int}\exp(-F\Psi/RT) \tag{27b}$$

with K_{a1}^{int} and K_{a2}^{int} as the intrinsic equilibrium constants which do not depend on surface charge. All reactants and products in the mass law equations which define the intrinsic surface complexations constants, K_{a1}^{int} and K_{a2}^{int}, are surface species:

$$K_{a1}^{int} = \frac{(\equiv SOH)\{H_s^+\}}{(\equiv SOH_2^+)} \tag{28a}$$

$$K_{a2}^{int} = \frac{(\equiv SO^-)\{H_s^+\}}{(\equiv SOH)} \tag{28b}$$

where H_s^+ denotes a proton released at the surface but not yet transported to the bulk solution.

The pH at which a mineral surface has zero net proton charge is named PZNPC (point of zero net proton charge). Since the proton charge arises from the ionisation of surface OH groups, the PZNPC is a characteristic parameter of the edge surface of montmorillonite. The PZNPC can be related to the intrinsic equilibrium constants by:

$$PZNPC = 0.5[pK_{a1}^{int} + pK_{a2}^{int}] \tag{29}$$

The generalized two-layer model presented by Dzombak and Morel (1990) is based on the diffuse double layer model (DDLM) (Stumm et al., 1970), but incorporates additional features. Dzombak and Morel (1990) successfully modelled the ionic strength dependent binding of cations and anions by incorporating different types of sites for surface complex formation. Furthermore, the improved version of the DDLM also accounts for surface precipitation at high cation and anion concentrations.

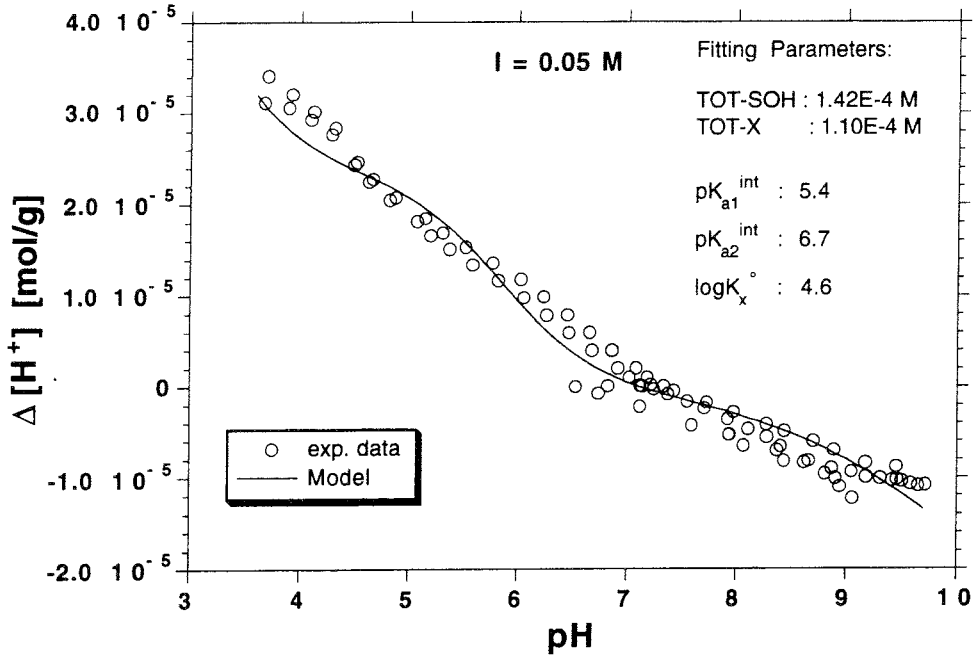

Figure 9 Titration curve of Na-montmorillonite (I = 0.05 mol/dm^3 $NaNO_3$, montmorillonite = 5 g/dm^3). Δ[H$^+$] corresponds to the protons bound on the mineral surface. The concentration of surface sites and the equilibrium constants are optimised for the experimental results.

4.2 *Evaluation of the model parameters for montmorillonite*

The surface chemical model for montmorillonite has been developed based on the following constraints: Montmorillonite reveals oxide-like behaviour in the alkaline pH range as indicated by the sequence of the protonation curves given in Figure 4. In the acid pH range, however, the acid/base characteristics of montmorillonite show the features of an exchanger phase typically found for clay minerals.

The model parameters required by the configuration of the diffuse double layer model are summarized in Table 2. The formal treatment of the pertinent protolysis reactions and ion exchange reactions is given by Eqs. (21) and (23). Fitting of the model parameters K_{a1}^{int} and K_{a2}^{int}, K_x°, TOT-SOH and TOT-X is performed with the least-square fit program GRFIT (Ludwig, 1992) which is an modified version of FITEQL (Westall, 1982). The model parameters were optimised for the experimental results determined

Table 2: Model parameters.

Model Parameters	SOH sites	X sites
Acidity constants: K_{a1}^{int} and K_{a2}^{int}	X	
H^+ - Na^+ exchange constant: K_x°		X
Total surface sites: TOT-site	X	X

Table 3: Summary of surface protolysis reactions and data for montmorillonite.

Surface protolysis reaction	Mass law equation	logK
$\equiv SOH_2^+ \Leftrightarrow \equiv SOH + H^+$	$K_{a1}^{int} = \frac{(\equiv SOH^o)\{H^+\}}{(\equiv SOH_2^+)} \exp(-\frac{F\Psi}{RT})$	-5.4±0.1
$\equiv SOH \Leftrightarrow \equiv SO^- + H^+$	$K_{a2}^{int} = \frac{(\equiv SO^-)\{H^+\}}{(\equiv SOH^o)} \exp(-\frac{F\Psi}{RT})$	-6.7±0.1
$H^+ + NaX \Leftrightarrow HX + Na^+$	$K_x^\circ = \frac{(x_{HX})(a_{Na})}{(x_{NaX})(a_H)}$	4.6±0.2
Site density TOT-SOH	2.8×10^{-5} mol/g	
Site density TOT-X	2.2×10^{-5} mol/g	

in a $NaNO_3$ medium of ionic strength I = 0.05 M (Figure 9). The relevant surface reactions, mass law equations and model parameters are summarised in Table 3.

The total number of variable-charge sites, TOT-SOH, obtained from the fitting procedure is 2.8×10^{-5} mol/g (2.8 meq/100 g) corresponding to about 2.6 % of the total CEC (108 meq/100 g). We estimate the specific surface area of the edge face to about 3 m^2/g, i.e., 9.5 % of the total BET surface area. Based on this assumption, the surface site density of OH groups amounts to 5.7 sites/nm^2. With an estimated specific surface area of 3 m^2/g, the resulting OH density on the edge surface of montmorillonite is within the range of the values typically obtained for oxide minerals. The total surface site density of oxid minerals ranges from 2 - 8 sites/nm^2 (Schindler, 1984; Wieland et al. 1988). The surface area of the basal planes hence results to 28.5 m^2/g (90.5%) of the external BET-surface area (31.53±0.16) m^2/g. Although the BET area of the edge face appears to be relatively large, the resulting OH density is reasonable and consistent with data reported in the literature.

The intrinsic acidity constants of the protolysis reaction (see Eqs. (23a) and (23b)) obtained from the fitting procedure are $pK_{a1}^{int} = (5.4 \pm 0.1)$ and $pK_{a2}^{int} = (6.7 \pm 0.1)$. The resulting PZNPC of the surface OH groups of Na-montmorillonite calculated with Eq. (29) is compared with values reported for K-montmorillonite, kaolinite and aluminum (hydr)oxides (Table 4). Although care should be taken when values given for the PZNPC from different investigators using different experimental and modelling approaches are compared, the PZNPC is a surface parmeter which yields information on the nature of the surface OH groups. Table 4 shows that the OH groups exposed at the surface of Na-montmorillonite are more acidic than aluminol surface sites but less acidic than silanol groups. From structural reasons, one expects surface silanol- and aluminol groups at the edge surface of montmorillonite. Our experimental results, however, can be interpreted by assuming only one type of surface OH groups. The discrepancy can be explained either as i) the occurrence of OH groups with intermediate acid/base characteristics at the edge surface of montmorillonite or ii) that Al(III) is adsorbed onto silanol groups and, hence, affects the acid/base characteristics of the silanol groups. Williams and Williams (1978) proposed a method for estimating the surface potential (i.e., zeta potential) of the edge surface of clay minerals. The authors assume that the surface potential can be approximated adequately by a linear combination of the potentials of the endmembers, i.e., quartz and alumina. For the edge surface of montmorillonite with Al and Si as the structure-forming constituents, one type of surface site with a PZNPC ~ 6 to 7 is predicted based on their surface model. Hence the theoretical PZNPC is in close agreement with our experimental value.

Table 4: Experimental values of the point of zero net proton charge (PZNPC) of mineral surfaces.

Mineral	PZNPC	Reference
Na-Montmorillonite	6.1	this study
K-Montmorillonite	7.8	Stadler and Schindler, 1993
K-Montmorillonite	5.9	Charlet et al., 1993
Kaolinite	7.5	Wieland and Stumm, 1992
γ- Al_2O_3	8.5	Huang and Stumm, 1973
α- Al_2O_3 (Corundum)	9.1	Sposito, 1984
α- $Al(OH)_3$ (Gibbsite)	9.1	Wieland et al., 1993
γ- $Al(OH)_3$ (Bayerite)	6.7	Pulfer et al., 1984
α- SiO_2 (Quartz)	2.9	Sposito, 1984

The total number of structural-charge sites, i.e., X layer sites, which are accessible for Na^+ - H^+ exchange reactions under the given experimental conditions is estimated to 2.2×10^{-5} mol/g (2.2 meq/100 g). This value is obtained from the fitting procedure. It corresponds to about 2.0% of the total CEC (CEC = 108 meq/100 g). We interprete the result as follows: Only a small fraction of layer sites are in equilibrium with the aqueous solution during the potentiometric titration of montmorillonite. The surface sites which are accessible for ion exchange reactions are probably exposed at the external planes. This is, most likely, a kinetic constraint imposed by limiting the equilibration period in the experiments to 10 min. A longer equilibration time would probably increase the fraction of structural-charge sites accessible for Na^+ - H^+ exchange reactions. The thermodynamic constant for the Na^+ - H^+ exchange is determined to $\log K^\circ_X = (4.6 \pm 0.2)$ indicating a strong affinity of the external X layer sites for protons. Note that the Na^+ - H^+ exchange constant derived in this study is comparable to the constant of the Na^+ - H^+ exchange at edge sites ($\log K^\circ_X = 4.0$) of montmorillonite as reported by Fletcher and Sposito (1989).

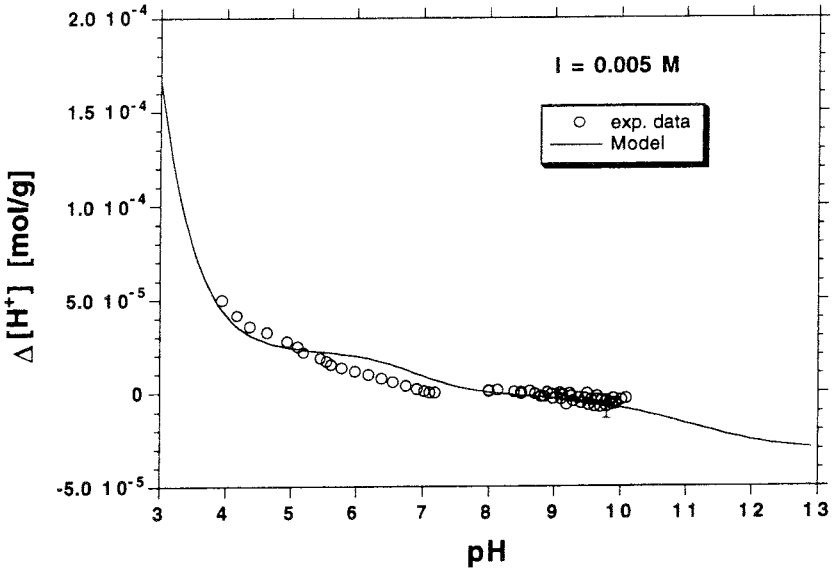

Figure 10a *Titration curve of Na-montmorillonite (I = 0.005 mol/dm^3 $NaNO_3$, montmorillonite = 5 g/dm^3). $\Delta[H^+]$ corresponds to the protons bound onto the montmorillonite surface. The solid line was calculated using the parameters listed in Table 3.*

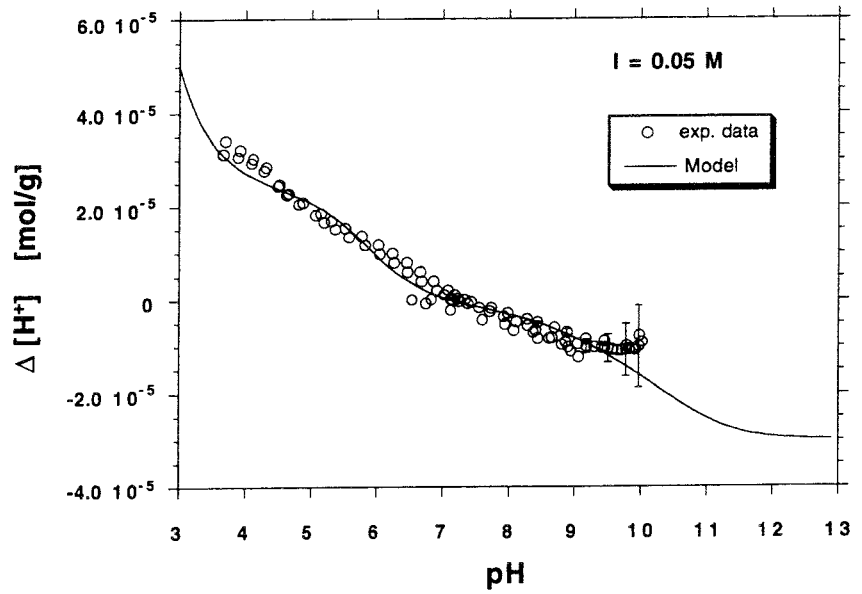

Figure 10b *Titration curve of Na-montmorillonite (I = 0.05 mol/dm^3 $NaNO_3$, montmorillonite = 5 g/dm^3). $\Delta[H^+]$ corresponds to the protons bound onto the montmorillonite surface. The solid line was calculated using the parameters listed in Table 3.*

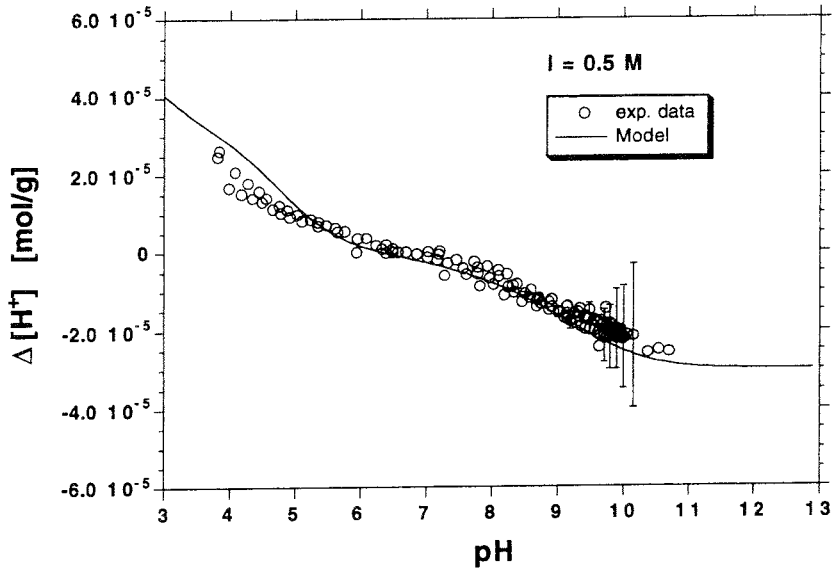

Figure 10c Titration curve of Na-montmorillonite (I = 0.5 mol/dm^3 $NaNO_3$, montmorillonite = 5 g/dm^3). $\Delta[H^+]$ corresponds to the protons bound onto the montmorillonite surface. The solid line was calculated using the parameters listed in Table 3.

4.3 *Modelling the acid/base behaviour of montmorillonite*

As shown in the previous section, the modelling parameters given in Table 3 result from the potentiometric titrations conducted at I = 0.05 M. The validity of the proposed model can be evaluated by predicting the total proton density at the montmorillonite surface, i.e., $\Delta[H^+]$, as a function of pH for I = 0.005 M and I = 0.5 M using the modelling parameters listed in Table 3. Note that the ionic strength is the only modelling parameter which has been changed in the computations displayed in Figures 10a and 10c. In Figures 10 a - c, model predictions (solid lines) and experimental data are compared for ionic strengths I = 0.005 M, I = 0.5 M and again for I = 0.05 M (see also Figure 9). Model predicition and experimental results agree very well in the alkaline pH range where surface OH groups are the only charge-determining surface sites. In this pH range, deprotonation of OH groups accounts for the total proton density, $\Delta[H^+]$, on the montmorillonite surface. Agreement between experimental results and model computation is less accurate but still satisfactory in the acid pH range. In the pH range < 7, both surface OH groups and layer sites control the surface proton density, $\Delta[H^+]$. Deviations between the predicted and experimental data in the

experiments conducted at I = 0.005 M and I = 0.5 M are likely due to the kinetic constraints imposed on the accessibility of the layer sites for Na/H exchange reactions. As mentioned above, the fraction of accessible structural-charge sites may depend on the equilibration time in the potentiometric titration experiments. Experimental evidence for a time dependence of the surface protolysis reaction has been provided in the case of kaolinite (Wieland and Stumm, 1992). Figures 10a - 10c show that the proposed two-site surface chemical model for montmorillonite adequately describes the pH dependence of surface protonation as observed in our experimental studies. A summary of all the experimental and modelling results is displayed in Figure 11.

The pH-dependent distribution of surface species under the given experimental conditions is shown Figures 12a - 12c. At the point of zero net proton charge of the edge surface (pH = 6.1), the concentration of protonated edge surface sites is equal to the concentration of deprotonated sites, i.e., $[SOH_2^+] = [SO^-]$. The ionic strength dependence of the protolysis degree of the surface sites is determined by the charge-potential relationship given in Eq. (26a). Hence the surface charge, i.e., the positive

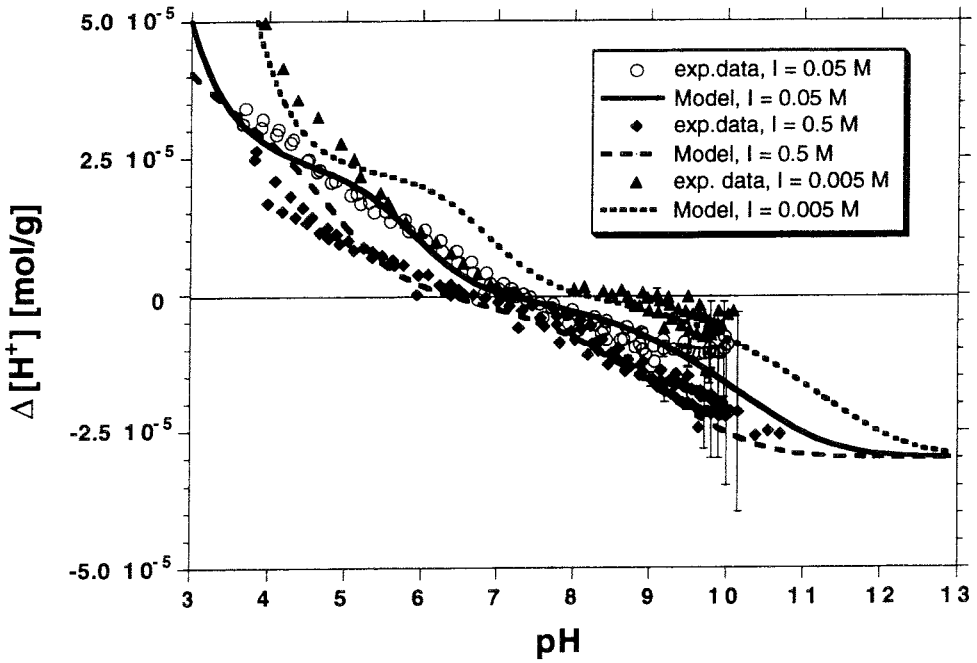

Figure 11 pH-dependent proton surface concentration, $\Delta[H^+]$, on Na-montmorillonite (5 g/dm^3). Experimental and modelling results are compared for ionic strengths I = 0.005 M, 0.05 M and 0.5 M. Model computations are performed using the parameters listed in Table 3.

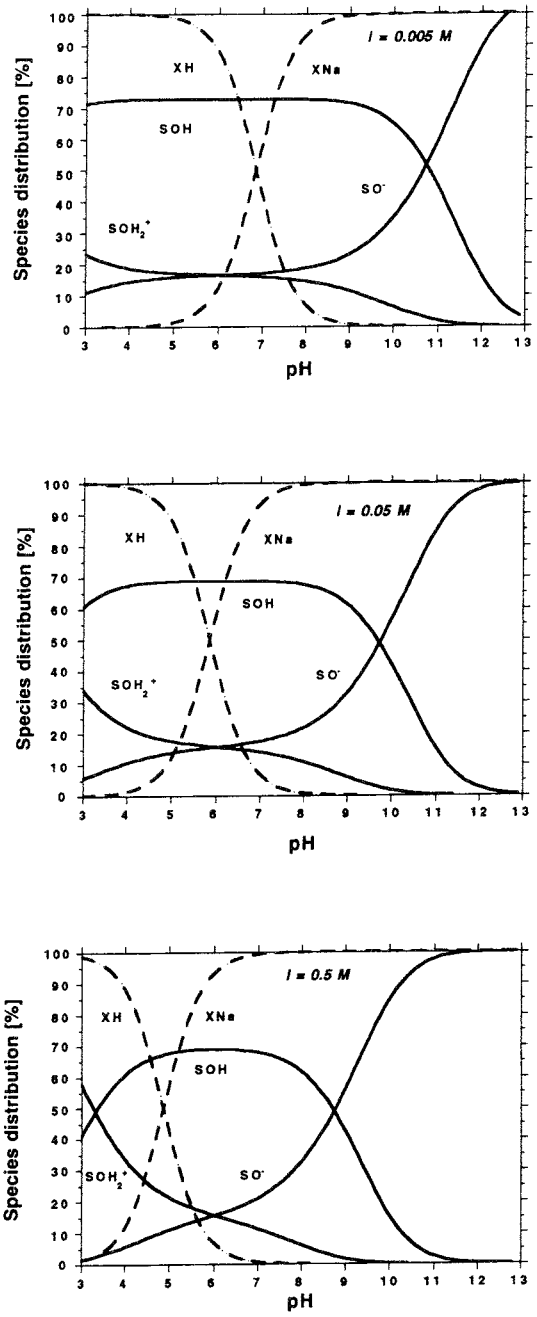

Figure 12 Species distribution at the montmorillonite surface for I = 0.005 mol/dm^3, I = 0.05 mol/dm^3 and I = 0.5 mol/dm^3. XNa and XH denote surface species of the X layer sites. SOH_2^+, SOH and SO^- are the protonated, neutral and deprotonated species of the surface OH groups, respectively.

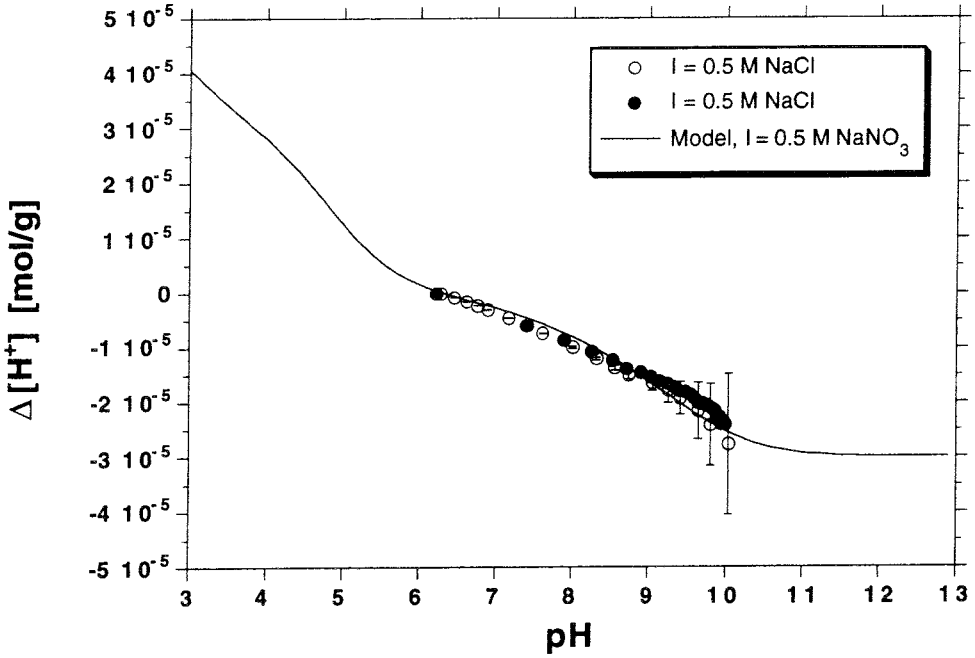

Figure 13 Titration curve of Na-montmorillonite. Data points are determined in 0.5 M NaCl. The solid line represents model computations for 0.5 M $NaNO_3$ using the parameters listed in Table 3.

charge below pH = 6.1 and the negative charge above pH = 6.1, increases with increasing ionic strength. Figures 12a - 12c also display the pH and ionic strength dependence of the Na^+ - H^+ exchange at X layer sites. Since the species distribution of X layer sites is controlled by the mass action law expressed in Eq. (22), the relative distribution of XNa and XH species is a function of the ionic strength. For example, the pH conditions where the concentrations of XNa and XH species are equal, i.e., [XNa] = [XH], depends on the concentration of the background electrolyte. The higher the concentration of the background electrolyte, i.e., the higher the ionic strength, I, the lower the pH where [XNa] = [XH] holds. An important feature revealed in Figures 12 a - c hence concerns the role of XH sites as source or sink for protons. Figure 12a, for example, indicates that, at low ionic strength, the X layer sites may significantly affect the proton balance in the alkaline and neutral pH range. At increased ionic strengths, i.e., I > 0.05 M, XH sites are relevant only at pH < 7.

Figure 13 displays the experimental data of two alkalimetric titrations conducted in suspensions using NaCl instead of $NaNO_3$ as background electrolyte. The solid line

represents model computations for a 0.5 M $NaNO_3$ background electrolyte using the parameters given in Table 3. Experimental data and model computations agree which is interpreted as evidence for the absence of ion-pair complex formation of chloride with ionisable surface sites. The experiments hence show that negatively charged OH groups are the only surface sites accounting for the interaction of protons with montmorillonite in the alkaline pH range. We also infer that the ionisation of surface OH groups is not affected by the nature of the anionic counterion, i.e., NO_3^- of Cl^-, of the background electrolyte.

4.4 A critical assessment of the validity of the proposed model

As outlined in the previous sections, the surface chemical properties of Na-montmorillonite as revealed in the potentiometric titration experiments of this study can be interpreted in terms of a two-site surface chemical model. OH groups (i.e., SOH sites) and structural-charge sites (X layer sites) are the surface functional groups exposed at the edge surface and at the external planes, respectively, accounting for the interaction of protons with the surface of montmorillonite. The total number of SOH groups and X layer sites are evaluated as fitting parameters. They are estimated to 2.8 mmol/100 g and 2.2 mmol/100 g which corresponds to 2.6 % and 2.0 %, respectively, of the CEC (108 meq/100 g). It shows that the fractions of surface sites accessible to protolysis reactions are small compared to the total number of available CEC sites.

Studies concerning the determination of the separate contributions of variable-charge and structural-charge sites are scarce. Anderson and Sposito (1991) recently investigated the separate contributions of variable-charge and structural-charge sites accessible to caesium exchange reactions on montmorillonite. At pH near 7, the total moles of caesium extracted from variable-charge and structural-charge sites were determined to (11.1 ± 2.9) mmol/100 g and (69.8 ± 3.7) mmol/100 g, respectively. The interaction of caesium with variable-charge surface sites is due to the formation of SO^-Cs^+ surface complexes. The concentration of SO^- sites as evaluated from the potentiometric titration of montmorillonite is significantly smaller. Figure 12 shows that, at pH near 7, about 20 % of the SOH sites are in the anionic form, corresponding to a SO^- concentration of 0.57 mmol/100g. The difference in the two estimates given for the concentration of SO^- sites at pH ≈ 7, i.e., 11.1 and 0.57 mmol/100 g, respectively, is most likely caused by experimental constraints. The measurement of separate contributions of OH groups (SOH edge sites) and structural-charge sites (X layer sites) as reported by Anderson and Sposito (1991) is an operational concept. The method uses differences in Cs^+ and Li^+ selectivity of siloxane surface (X layer sites)

and ionisable surface groups (SOH edge sites) as measure to quantify the fraction of surface sites. It is assumed that Li^+ selectively displaces Cs^+ bound as SO^-Cs^+ surface complex, without displacing Cs^+ associated with siloxane sites. However, this operational concept based on selectivity may overestimate the total number of OH groups due to interaction of Li^+ with structural-charge sites. Differences in the values for the total number of surface OH groups may simply reflect differences in the procedures for estimating the OH group densities.

The number of X layer sites in equilibrium with the aqueous solution has been estimated to 2 % of the CEC. As mentioned above, the number of X layer sites acting as reactive sites in Na^+ - H^+ exchange reactions may be time-dependent and, hence, determined by the kinetic constraints imposed on the experiment. A potentiometric-titration study of a "Cerro Bandera" montmorillonite was recently conducted by Avena et al. (1990). NaCl was used as background electrolyte at total concentrations of 0.01 and 0.1 M. The samples were equilibrated for 30 min. Figure 14 compares the experimental results of our study (I = 0.05 M) with the results reported by Avena et al. (1990) (I = 0.01 M and = 0.1 M).

Figure 14 shows that Avena et al. (1990) observed an enhanced surface proton concentration, $\Delta[H^+]$, in the acidic pH range. The experimental results of the two studies are consistent in the alkaline pH range. The higher concentration of surface protons in the study of Avena et al. (1990) may partially be attributable to the origin of the clay minerals. In both studies, however, similar procedures were used to prepare a <2 µm fraction of the homoionic Na-form. The cation exchange capacities (CEC) are comparable, i.e., 91.7 and 108 meq/100 g, respectively. Therefore we expect that the physico-chemical characteristics of Wyoming and Cerro Bandera montmorillonite are similar. We hence infer that increasing the equilibration period from 10 min (our study) to 30 min (Avena et al., 1990) could account for the enhancement in the surface proton concentration in the study of Avena et al. (1990). It appears that the longer the equilibration period is, the more layer sites are accessible to Na^+ - H^+ exchange.

Figure 14 further reveals that although the two-site model with SOH groups and X layer sites as the reactive surface ligands predicts the pH dependence of the surface proton or hydroxyl concentration, $\Delta[H^+]$, in our experimental studies (Figures 9, 10 and 11), it underestimates the extent of proton adsorption at pH < 7 on montmorillonite as reported by Avena et al. (1990). In order to adequately mimic the experimental data at pH < 7 in the study of Avena et al. (1990), an extension of the proposed two-site model is

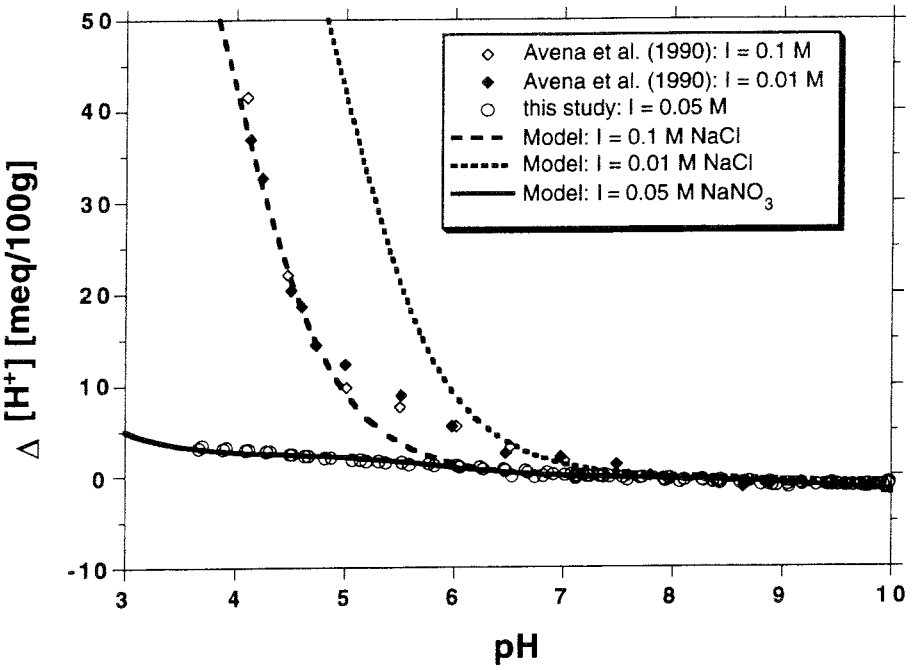

Figure 14 Potentiometric titration curves for Na-montmorillonite. Results of our study (circles) measured at I = 0.05 M $NaNO_3$ (montmorillonite = 5 g/dm^3, t = 22 °C, equilibration time = 10 min) are compared with the experimental data (squares) taken from Avena et al. (1990) (I = 0.1 M and 0.01 M NaCl, montmorillonite = 0.5 - 0.6 g/dm^3, t = 30°C, equilibration time = 30 min). The solid line represents model computations for 0.05 M $NaNO_3$ using the parameters listed in Table 3. Broken and dotted lines show modelling calculations assuming a three-site surface chemical model with SOH groups (edge sites) and two layer sites (denoted as X and Y layer sites) as the reactive surface functional groups. The modelling parameters for the edge and X layer sites are listed in Table 3. The modelling parameters for the Y layer sites are: TOT-Y (= CEC) = 91.7meq/100g, $\log K_x^\circ$ = 3.0.

required. We therefore introduce a second type of layer sites, denoted as Y layer sites, accounting for the reactivity of the bulk of structural-charge sites. The X layer sites introduced in our study are attributable to layers sites exposed at the external surface. Y layer sites, however, denote the layer sites located at the internal surface of a montmorillonite platelet. The total density of Y layer sites and the Na^+ - H^+ exchange constant used in the model computations are given by: TOT-Y (= CEC) = 91.7

meq/100g, $\log K^{\circ}_{X}$ = 3.0. The value for the CEC has been reported by Avena et al. (1990). The equilibrium constant, $\log K^{\circ}_{X}$ = 3.0, is a fitting parameter derived from an optimisation of our model for the experimental data presented by Avena et al. (1990). Figure 15 shows that the proposed three-site model correctly predicts the experimentally observed increase in the surface proton density, $\Delta[H^+]$, below pH = 5 for I = 0.1 M. At low ionic strength, however, the model calculations overestimate ionic strength effects. A detailed evaluation of the discrepancy between our model predictions and the experimental data obtained for Cerro Bandera montmorillonite at low ionic strength requires an extension of the experimental programme for Wyoming bentonite in order to validate the surface chemical model in the acidic pH range.

The Na^+ - H^+ exchange constant ($\log K^{\circ}_{X}$ = 3.0) for Y layer sites is lower than the exchange constant estimated for X layer sites ($\log K^{\circ}_{X}$ = 4.6). High values for $\log K^{\circ}_{X}$ indicate a strong affinity of protons for layer sites. Values for the Na^+ - H^+ exchange constants published in the open literature are scarce. Schindler et al. (1987) investigated the acid/base characteristics of kaolinite using a potentiometric titration technique. Since both montmorillonite and kaolinite are layer silicates with siloxane cavities as the reactive surface functional groups involved in ion exchange reactions (Sposito, 1984), the Na^+ - H^+ exchange constants for montmorillonite and kaolinite can be compared. Schindler et al. (1987) reported a value of $\log K^{\circ}_{X}$ = 2.9 for the Na^+ - H^+ exchange constant on kaolinite which is in agreement with our value derived for Wyoming bentonite ($\log K^{\circ}_{X}$ = 3.0). Note that 2:1 phyllosilicates are supposed to be present as impurities in kaolinite.

Fletcher and Sposito (1989) evaluated the constants for ion exchange reactions on montmorillonite from a range of sources (see references therein) and "in conjunction with simplifying assumptions" to generate a consistent, but "preliminary", database. TheNa^+ - H^+ exchange constant on montmorillonite given by Fletcher and Sposito (1989) is $\log K^{\circ}_{X}$ = 0.15. The inconsistency of the Na/H exchange constants obtained in our study ($\log K^{\circ}_{X}$ = 3.0) and those reported by Fletcher and Sposito (1989) ($\log K^{\circ}_{X}$ = 0.15) cannot be explained based on the present knowledge and the experimental data available in the literature.

If it is admitted that the proposed three-layer model is an appropriate modelling tool for describing protolysis reactions at the montmorillonite water/interface, we can estimate the effect of the Na^+ - H^+ exchange at Y layer sites on the experimental results

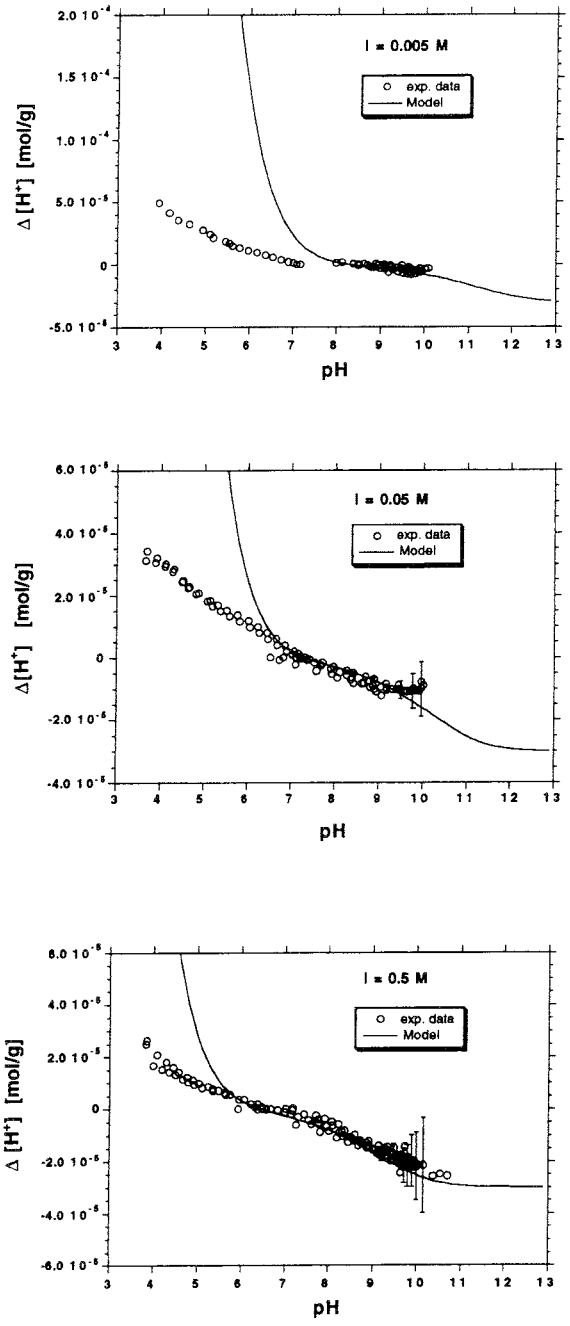

Figure 15 Potentiometric titration curves for Na-montmorillonite. The solid lines represent model computations based on a three-site model with surface OH groups and two layer sites as the surface functional groups. The modelling parameters for the OH groups and X layer sites are listed in Table 3. The parameters for the second type of layer site, i.e., Y layer sites, are: TOT-Y = 105.8 meq/100 g and $\log K^{\circ}_{x} = 3.0$.

obtained in our study. In the following model calculations, we assume that Y layer sites are in equilibrium with the aqueous solution. The model computations are performed using the parameters for SOH and X layer sites as listed in Table 3. The modelling parameters for Y layer sites are: TOT-Y = 105.8 meq/100 g (= CEC - TOT-X) and $\log K^{\circ}_{x}$ = 3.0. In Figures 15a - 15c, the experimental data obtained in our study are compared with the results from model computations (I = 0.005 M, 0.05 M and 0.5 M $NaNO_3$). If Y layer sites were in equilibrium with the aqueous solution in our experiments, one should observe a significant increase in the concentration of surface protons in the pH range 5.5 - 7.5 depending on the concentration of the background electrolyte. For I = 0.005 M $NaNO_3$, the exchange of Na with protons is predicted to occur already in the pH range 7 - 8. At moderate and high ionic strengths, a significant exchange of Na with protons should only occur below pH $\approx$ 6.5. Figures 15a - 15c clearly indicate that the experimental results obtained in the alkaline pH range can be interpreted equally well using either the two-site or the three-site model. Under repository conditions, pH values > 7 are expected in the porewater of compacted bentonite. Therefore, we may infer that the proposed two-site model for montmorillonite adequately describes the acid/base properties of bentonite for the geochemical conditions encountered in a repository for radiocative waste.

5 Near field chemistry under repository conditions

5.1 Prediction of the porewater chemical composition in compacted bentonite

Compacted bentonite is envisaged as containment barrier for the disposal of radioactive waste. The characteristics of the bentonite backfill material used in the Swedish disposal scenario are summarised in Table 5. The values given in Table 5 are based on a previous study by Wanner et al. (1992) reporting the thermodynamic modelling of the bentonite/groundwater interactions encountered in Swedish repositories. The cation exchange capacity (CEC) is adjusted to 85 meq/100 g according to the measurements made on untreated bulk material of Wyoming MX-80 bentonite instead of 76.4 meq/100 g as given by Wanner et al. (1992). The percent distribution of the exchangeable cations and the content of impurities are reported by Wanner et al. (1992).

As mentioned in the previous section, the surface chemical model for montmorillonite is based on experimental studies conducted at a low bentonite/water ratio, i.e., b/w = 0.005 kg/dm^3. Extrapolation of the bentonite model to higher compaction degrees, i.e., higher bentonite/water ratios, thus includes the following assumptions:

1) The thermodynamic equilibrium constants for ion exchange and surface protolysis reactions are valid irrespective of the degree of compaction of bentonite.
2) The total number of OH surface sites and the CEC are proportional to the solid content.

The first assumption implies that the reactivity of surface sites, i.e., OH surface functional groups and ion exchange sites, is not affected by the bentonite/water ratio. The second assumption indicates that the accessibility of both types of surface sites i.e., OH surface functional groups and ion exchange sites, is proportional to the bentonite/water ratio regardless of the compaction degree of bentonite.

The characteristic parameters for bentonite are listed in Table 5. Na^+, Ca^{2+} and Mg^{2+} are the main cations which interact with X and Y sites of montmorillonite. Since the amount of K^+ adsorbed on montmorillonite is small, i.e. 0.3 %, its effect on porewater chemistry is not of importance in the model computations. Therefore, and in order to achieve consistency with the model computations of Wanner et al. (1992), ion exchange reactions of this cation are not considered in the present model. The proportion of Na^+, Ca^{2+} and Mg^{2+} associated with X and Y layer sites are assumed to be equal for both types of ion exchange sites. Na^+ is the dominant counterion of the ion-exchange sites

indicating that the Na-form of montmorillonite is the main component of bentonite. Wyoming Mx-80 bentonite contains impurities of quartz (10 %), calcite (1.4 %) and small amounts of $CaSO_4$ (0.34 %) and NaCl (0.0067 %) (Table 5).

We predict the chemical composition of porewater in compacted bentonite for increasing degree of compaction of bentonite (Figure 16). The model is based on the following assumptions:

- Na-bentonite (MX-80) reacts with Allard groundwater whose chemical composition is given in Table 6.
- The surface chemical model for montmorillonite comprises the surface reactions given in Table 7.
- Quartz and calcite saturation is reached according to a closed system.
- $CaSO_4$ and NaCl impurities completely dissolve.

Changes in the chemical composition of groundwater reacting with bentonite are calculated for increasing contents of bentonite in solution which is expressed as increasing ion exchange capacity in the system. The cation exchange capacity ranges from 10^{-4} eq/dm^3 to 10 eq/dm^3 (Figure 16a and 16b) which corresponds to bentonite/water ratios ranging from 1.2×10^{-4} kg/dm^3 to 12 kg/dm^3. The surface chemical model for montmorillonite is established based on experiments conducted in suspensions of low bentonite/water ratios, i.e., 5×10^{-3} kg/dm^3 or CEC = 4.25×10^{-3} eq/dm^3, respectively. The extrapolation to chemical conditions in the near field is straightforward and includes the assumptions mentioned above. The chemical composition of porewater in compacted sodium bentonite corresponds to the composition indicated at CEC = 3.9 eq/dm^3 (Figure 16a and 16b).

The effect of increasing compaction of bentonite on the pH of the porewater is illustrated in Figure 16a. For near-field conditions, the pH value of the porewater is estimated to 7.3. According to the model calculations, the protolysis reactions at the edge sites of montmorillonite compensate the pH increase caused by calcite dissolution in a calcite saturated bentonite/groundwater system (Wanner, 1985). Under the given chemical conditions, about 2×10^{-2} mol/dm^3 $CaCO_3$ and 1×10^{-4} mol/dm^3 SiO_2 are dissolved. The concentrations of Na^+, Ca^{2+} and Mg^{2+} in porewater are controlled by ion exchange reactions occurring at the layer sites of montmorillonite. In Figure 16b, the distribution of the surface sites involved in proton exchange reactions is displayed as a function of the CEC of the bentonite/water system. The percent distribution relates the concentration of SOH_2^+, SO^- and XH sites to the total concentration of edge sites,

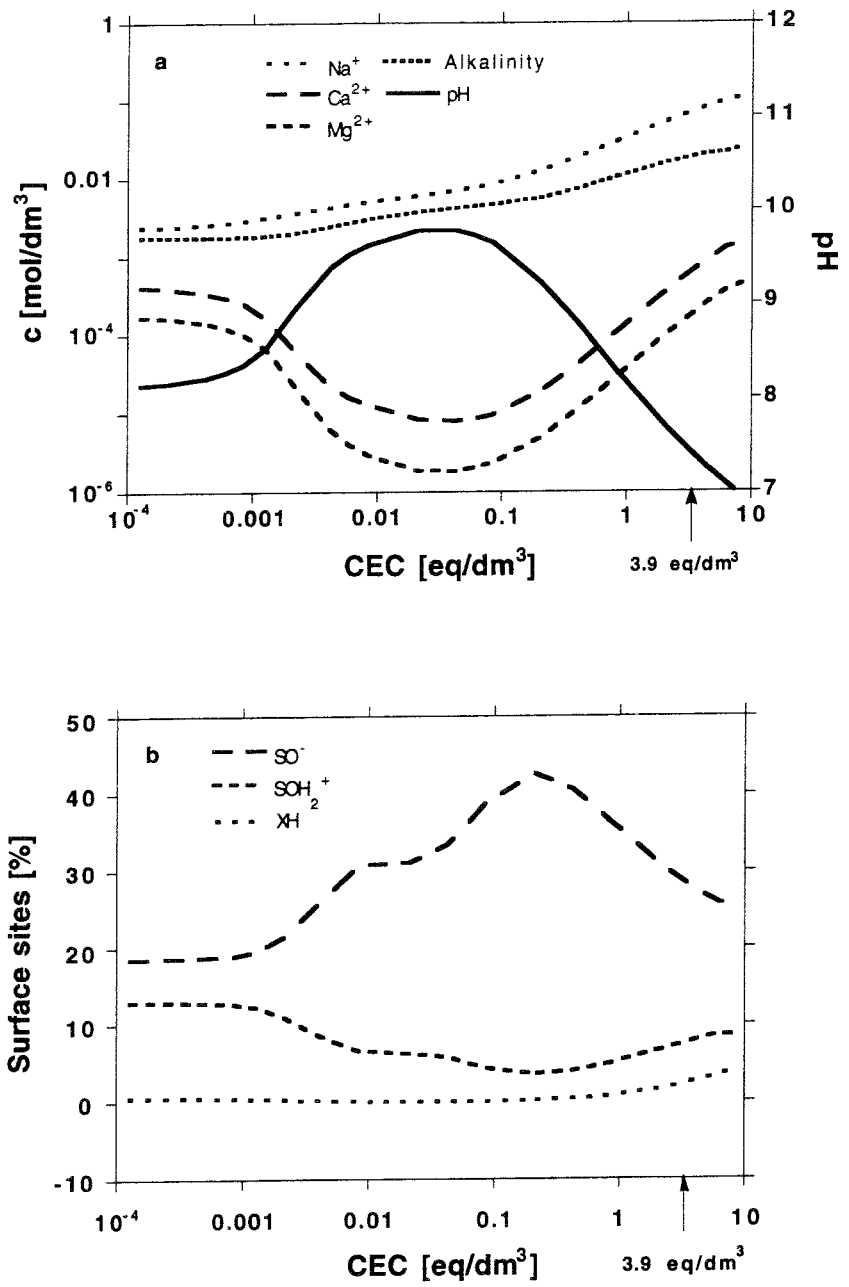

Figure 16 The effect of the degree of compaction of bentonite on the chemical composition of porewater (above) and the distribution of surface sites (below) when Allard groundwater is equilibrated with bentonite. The degree of compaction is represented by the total concentration of ion-exchange sites, i.e., the concentration of X + Y layer sites. Alkalinity is expressed in eq/dm^3. Na^+, Ca^{2+} and Mg^{2+} indicate the concentration of the free cation in solution. SOH_2^+ and SO^- represent the protonated and deprotonated edges sites. XH denotes protonated layers sites. The CEC in compacted bentonite corresponds to 3.90 eq/dm^3.

Table 5: Data for Wyoming MX-80 bentonite used for modelling near-field conditions.

Property	Value	Reference [a]
Cation Exchange Capacity (CEC) [b]	85.0 meq/100 g	this study
External layer sites (X sites)	1.7 meq/100 g	this study
Internal layer sites	83.3 meq/100 g	this study
Edge sites (OH groups)	2.8 meq/100 g	this study
Exchangeable Na [b]	81.7 %	2
Exchangeable Mg [b]	3.9 %	2
Exchangeable Ca [b,c]	14.1 %	2
Total carbonate ($CaCO_3$)	1.4 % (wt)	2
Total quartz (SiO_2)	10 % (wt)	3
NaCl impurities	0.007 %	1
$CaSO_4$ impurities	0.34 %	1
Density (highly compacted)	1.70 g/cm^3	4
Density (highly compacted, water saturated)	2.07 g/cm^3	4
Porewater/bentonite ratio	0.38 cm^3/cm^3	5

a) References: 1: Wanner et al. (1992), 2: Müller-Vonmoos and Kahr (1985), 3: van Olphen and Fripiat (1979), 4: McKinley (1984), 5: Project Gewähr (1985).

b) The values refer to 100 g oven-dried material. The contribution of K is small, i.e., 0.3 %, and, therefore, neglected in the present model computations.

c) The value for exchangeable Ca should be subject to systematic error because of the presence of calcite

Table 6: The chemical composition of Allard water (simplified).

	Concentration [mol/dm^3]
Na^+	2.26E-3
Ca^{2+}	4.64E-4
Mg^{2+}	1.90E-4
Cl^-	1.48E-3
SO_4^{2-}	1.00E-4
alkalinity	1.80E-3
pH	8.1
ionic strength	4.3E-3

Table 7: Surface chemical equilibria.

Surface reactions			logK	Reference
$\equiv SOH_2^+$	$\Leftrightarrow$	$\equiv SOH + H^+$	-5.4	this study
$\equiv SOH$	$\Leftrightarrow$	$\equiv SO^- + H^+$	-6.7	this study
$H^+ + NaX$	$\Leftrightarrow$	$HX + Na^+$	4.6	this study
$Ca^{2+} + 2\ NaX$	$\Leftrightarrow$	$CaX_2 + 2\ Na^+$	0.21	Wanner et al., 1992
$Mg^{2+} + 2\ NaX$	$\Leftrightarrow$	$MgX_2 + 2\ Na^+$	0.13	Wanner et al., 1992
$H^+ + NaY$	$\Leftrightarrow$	$HY + Na^+$	3.0	this study
$Ca^{2+} + 2\ NaY$	$\Leftrightarrow$	$CaY_2 + 2\ Na^+$	0.21	Wanner et al., 1992
$Mg^{2+} + 2\ NaY$	$\Leftrightarrow$	$MgY_2 + 2\ Na^+$	0.13	Wanner et al., 1992

SOH groups (TOT-SOH = 2.84×10^{-5} mol/g), and external layer sites, i.e., X groups (TOT-X = 2.2×10^{-5} mol/g). Figure 16b emphasizes the key role of edge sites in controlling the pH of porewater in compacted bentonite. The external layer sites, i.e., X sites are of minor importance, and the internal layer sites, i.e., Y sites are not relevant as either proton source or sink in the alkaline pH range. For example, at CEC = 3.9 eq/dm^3, only 2.4 % of X sites exist in the protonated form, XH. Due to the even lower affinity of the Y layer sites for protons, the concentration of the YH form is negligibly small. The ratio of SOH_2^+ and SO^- in Figure 16b depends on pH and the concentration of the ionic background medium (see Section 4.1). With increasing compaction of bentonite, the ionic strength increases from originally 3×10^{-3} mol/dm^3 at CEC = 1×10^{-4} eq/dm^3 to 0.26 mol/dm^3 at CEC = 3.9 eq/dm^3 due to the dissolution of impurities. Since both parameters change with increasing bentonite compaction, i.e., pH and ionic strength, their effects on the protonation reactions occurring at edge sites superimpose in the model computations presented in Figure 16b.

It is worthwhile mentioning that the model computations presented in Figures 16a and 16b are based on a CEC of 85 meq/100g determined for dispersed bentonite. The effective CEC observed under near-field conditions is likely diminished due to compaction of bentonite. The loss of available CEC sites in compacted bentonite is also reflected in a decrease in the porosity with increasing degree of compaction. Since it is impossible to adequately evaluate the number of available exchange sites in compacted bentonite at present, we assumed the maximum number of sites as representative estimate for the CEC of bentonite under near-field conditions.

5.2 *Comparison of model computations with experimental data for high bentonite/water ratios*

The proposed bentonite model was used to predict the porewater composition of compacted bentonite in experiments carried out by Werme (1992) and communicated to Wanner et al. (1992). The experiments were conducted in suspensions with 1.4 g bentonite per cm^3 water. A few hundred microliters of porewater were sampled after equilibrating bentonite with deionised water and Allard groundwater. Sampling was performed by squeezing the suspension under high pressure (Werme, 1994). Measured concentrations of the main constituents, i.e. Ca^{2+}, Mg^{2+}, Na^+, SO_4^{2-}, Cl^-, as well as pH and alkalinity (Alk) are listed in Table 8. The chemical composition of the porewater is predicted assuming that untreated Wyoming MX-80 bentonite

Table 8: Experimental and modelled data of the solution composition after reaction of Na-bentonite with deionised and Allard water. The solid/water ratio is 1.4 g/cm^3. Values correspond to total concentration in solution in M (mol/dm^3), except Alk (eq/dm^3).

Exp.		TOT-Na	TOT-Ca	TOT-Mg	Cl^-	SO_4^{2-}	Alk	pH
deionised water								
56/57	exp.	1.0E-1	1.5E-4		1.5E-3	4.0E-2	1.0E-2	9.2
62/63	exp.	8.3E-2	1.0E-4		1.5E-3	3.5E-2	4.3E-3	9.0
	model	7.6E-2	1.4E-3	3.9E-4	1.6E-3	3.0E-2	3.4E-3	8.4
Allard water								
58/59	exp.	9.4E-2	4.5E-4	4.1E-6	1.8E-3	3.3E-2	5.5E-3	9.2
60/61	exp.	8.9E-2	1.0E-4		1.7E-3	3.2E-2	6.5E-3	9.0
	model	7.7E-2	1.4E-3	3.9E-4	1.7E-3	3.0E-2	3.4E-3	8.4

is in equilibrium with deionised water or groundwater in an open system ($pCO_2 = 10^{-3.5}$ atm). The results reported for soda-treated bentonite are not modelled, since important details of the preparation of soda-treated bentonite are not known (Wanner et al., 1992). Again, the model predictions are based on the surface equilibria and the parameters for bentonite as summarised in Tables 5 and 7.

Experimental and modelled concentrations of the main constituents are compared in Table 8. Predictions and measurements are consistent within the validity of the model and given the fact that uncertainties in the experimental method may exist. Agreement between experimental and predicted concentrations are found for chloride and sulfate indicating dissolution of NaCl and $CaSO_4$ impurities. Significant deviations are found for the total concentrations of calcium and for pH. The predicted pH value is lower than the experimental data. The pH value depends to a large extent on the amount of soluble impurities and their availability for dissolution into the aqueous phase. The model uses

an inventory of soluble impurities which was derived from Werme's experiments and which is subject to uncertainties. In addition, the model assumes instantaneous dissolution of all soluble impurities into the aqueous phase. This assumption is also uncertain, but there is no quantitative information available allowing a verification of this assumption. In this light the deviation of the predicted pH values from the experimental ones is not considered serious. The calculated Ca concentration, on the other hand, is about a factor of ten higher than the experimental data. The discrepancy in the Ca concentration is only partially attributable to a decrease in the solubility of calcite with increasing pH, since the formation of $CaSO_4$ complexes in solution is relevant in media with high sulfate concentrations. The concentration of $CaSO_4$ complexes in solution can be estimated to about 7×10^{-4} M for a given total sulfate concentration of 3×10^{-2} M. Since the sulfate concentrations in the experiments are even higher, the total concentrations of calcium in the experiments should exceed 7×10^{-4} M. Table 8 shows, however, that the experimentally determined Ca concentrations are significantly lower. The discrepancy between the model computations and the experiments can be explained in view of the equilibrium situation involving ion exchange and calcite solubility: Compared to the model calculations, the ion exchange equilibrium is shifted towards increased calcium sorption in the experiments giving rise to a decrease in the calcium and an increase in the sodium concentrations in solution. Adjustment of the calcite equilibrium then leads to increases in alkalinity and pH. With the aid of the bentonite model, the equilibrium situation as observed in the experiments can be correctly predicted simply by increasing the Na^+ - Ca^{2+} exchange constant by 1.5 log units. One may envisage that sampling of the porewater at elevated pressure could impose modified equilibrium conditions and, hence, explain the discrepancy between experimental data and model computations. However, in order to enlighten the discrepancy between the modelled and experimentally determined equilibrium situation, critical assessments of both the validity of the bentonite model and the effect of sampling techniques on chemical equilibria in compacted bentonite are required.

We therefore infer that testing the bentonite model based on the experiments conducted by SKB (Werme, 1992) allows no final conclusions regarding the validity of the model. Methodical constraints are imposed on both methods for evaluating the chemical composition of porewater in compacted bentonite, i.e., model computations and experiments. The effect of compaction on the number of available surface sites in the modelling approach and the suitability of the sampling technique in the experiments should be addressed in a thorough validation procedure. We therefore recommend that further validation of the bentonite model should be envisaged in combination with additional experimental studies.

5.3 *Long-term extrapolations: Mixing tank model*

5.3.1 *Derivation of the mixing tank model*

Wanner (1986) and Wanner et al. (1992) used a mixing tank model in order to estimate the effect of time on the near field chemistry under repository conditions. The main assumptions behind the model are:

1) Complete mixing of groundwater flowing past the repositiory with the near-field water
2) Uniformity of the composition of porewater throughout the near field

Time dependence of the porewater evolution is expressed in terms of water exchange cycles. A water exchange cycle is defined as a complete replacement of the bentonite porewater with fresh groundwater. Wanner et al. (1992) estimate the timescale for one water exchange cycle to 13'800 years for the Swedish repository design. The timescale is based on the assumption that the water in the interlamellar spaces of montmorillonite is also replaced.

5.3.2 *Long-term predictions using the mixing tank model*

Long-term calculations are done as reported by Wanner et al. (1992) using an extended version of the code MIN_SURF. They are made for compacted bentonite in contact with Allard and Äspö groundwater. The chemical compositions of the groundwaters are listed in Tables 6 and 9.
In a first step, the equilibrium conditions for fresh Wyoming MX-80 bentonite in contact with Allard and Äspö groundwater is calculated. For Allard groundwater, the initial equilibrium situation correspond to the chemical conditions given in Figure 16a at a CEC of 3.9 eq/dm^3. In the following, the code calculates the composition of porewater and the relative proportion of exchangeable cations on bentonite for each exchange cycle. After each exchange cycle, fresh groundwater is assumed to be in contact with compacted Wyoming MX-80 bentonite. The exchange procedure is repeated 200 times.

In Figure 17, the evolution of the porewater composition for bentonite in contact with Allard groundwater as well as the relative portion of surface sites on bentonite is

Table 9: The chemical composition of Äspö water (simplified).

	Concentration [mol/dm^3]
Na^+	1.31E-1
Ca^{2+}	1.10E-1
Mg^{2+}	2.06E-3
Cl^-	3.40E-1
SO_4^{2-}	7.40E-3
alkalinity	1.80E-4
pH	7.4
ionic strength	4.60E-1

presented as a function of water exchange cycles. Na(X/Y), $Ca(X/Y)_2$, $Mg(X/Y)_2$ and H(X/Y) denote the association of the corresponding cations or the proton, respectively, with X and Y layer sites. The results of the calculations are listed in Table 10. After 90 exchange cycles, the calcite pool of the bentonite backfill material is depleted. According to the present mixing tank calculations, the initial pH of the porewater is predicted to be much lower than reported in previous studies (Wanner, 1986; Wanner et al., 1992). In the previous model calculations (Wanner, 1986; Wanner et al., 1992), the initial pH was predicted to be around 10.5 after the first exchange cycle indicating pH control by calcite solubility in a closed system. By incorporating the acid/base characteristics of edge surface sites in the model, a pH value of 8.4 is reached. The pH value drops to about pH = 7.1 after complete removal of calcite from bentonite, and, hereafter, slowly decreases with time to about pH = 6.8. The drop in pH coincides with a decrease in the alkalinity.

As stated by Wanner et al. (1992), the dissolution of calcite and the transformation of Na-bentonite to a Ca-rich bentonite are the main features of the long-term predictions. The following reaction summarises the transformation of sodium into calcium bentonite:

$$2\ Na(ex) + CaCO_3 + H^+ \Leftrightarrow Ca(ex) + 2\ Na^+ + HCO_3^-$$

Calcite dissolution hence provides a continuous source of calcium to the porewater. The process results in a slow exhaustion of the calcite pool.
The transformation of Na-bentonite to a Ca-rich bentonite in contact with Allard groundwater is displayed in Figure 17. Na^+ and Ca^{2+} are the dominant exchangeable cations for both X and Y layer sites on bentonite under the given repository conditions. The amounts of exchangeable Mg^{2+} and H^+ on layer sites are minor. Hence, in the case of Allard groundwater, the transformation of bentonite is critically dependent on the amount of available calcite. The final Ca/Na ratio on bentonite is predicted to about 3/2. The edge surface of montmorillonite is negatively charged, i.e., the concentration of SO^- sites slightly exceeds those of SOH_2^+.

The higher concentrations of Na^+, Ca^{2+} and Cl^- in Äspö groundwater significantly affect the long-term evolution of the porewater composition in the near field. The results of the calculations are listed in Table 11. Depletion of calcite occurs over a longer period of time, i.e., about 190 instead of 90 exchange cycles. During depletion of calcite, the pH of the porewater is predicted to about pH = 6.5. It drops to about pH = 6 after exhaustion of the calcite pool. Again, pH is controlled by protolysis reactions occurring at the edge surface of montmorillonite and by calcite dissolution. In Äspö groundwater, the transformation of Na-bentonite to Ca-bentonite occurs within 40 exchange cycles. Hence, calcite plays a minor role in the transformation process in highly mineralised groundwaters.

The present model computations indicate that both the dissolution of calcite and the acid/base characteristics of OH sites at the montmorillonite surface control pH and alkalinity of the porewater in the near field. In the previous studies of the near field chemistry in a repository reported by Wanner (1986) and Wanner et al. (1992), chemical interactions at the mineral/water interface were ascribed to cation exchange reactions with layer and edge sites. In those studies, pH and alkalinity were controlled by calcite dissolution in a closed system. Both the present study and the previous studies predict the transformation of Na-bentonite to a Ca-rich bentonite. As shown in this work, the bentonite transformation is accelerated in the presence of the highly mineralised Äspö groundwater.

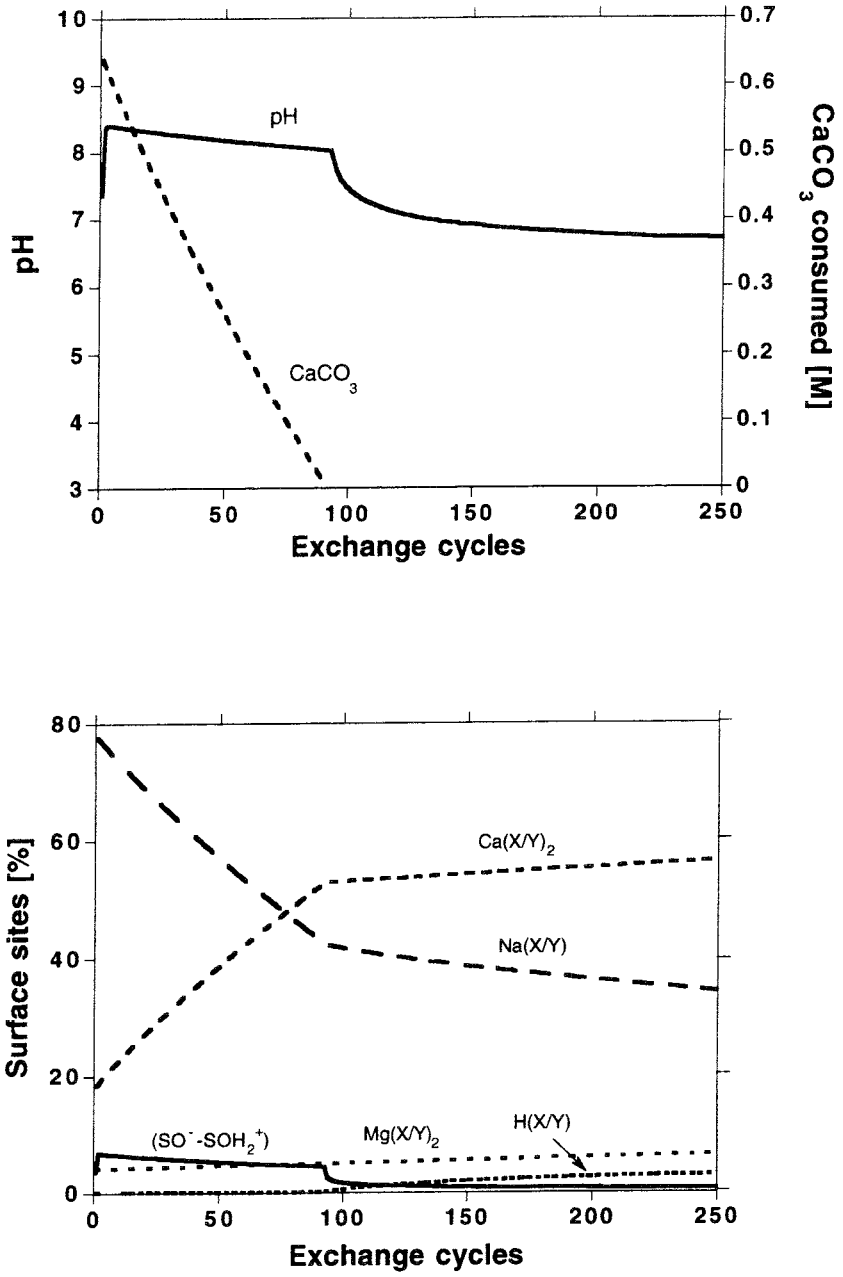

Figure 17 Bentonite in contact with Allard groundwater. Prediction of pH, consumed calcite, exchangeable ions (Na^+, Ca^{2+}, Mg^{2+}, H^+) and negatively charged edge sites (SO^- - SOH_2^+) as a function of exchange cycles according to the mixing tank model. Two types of layer sites, X and Y, are considered in the model computations (see text). The composition of Allard groundwater is given in Table 6. The surface chemical reactions are listed in Table 7.

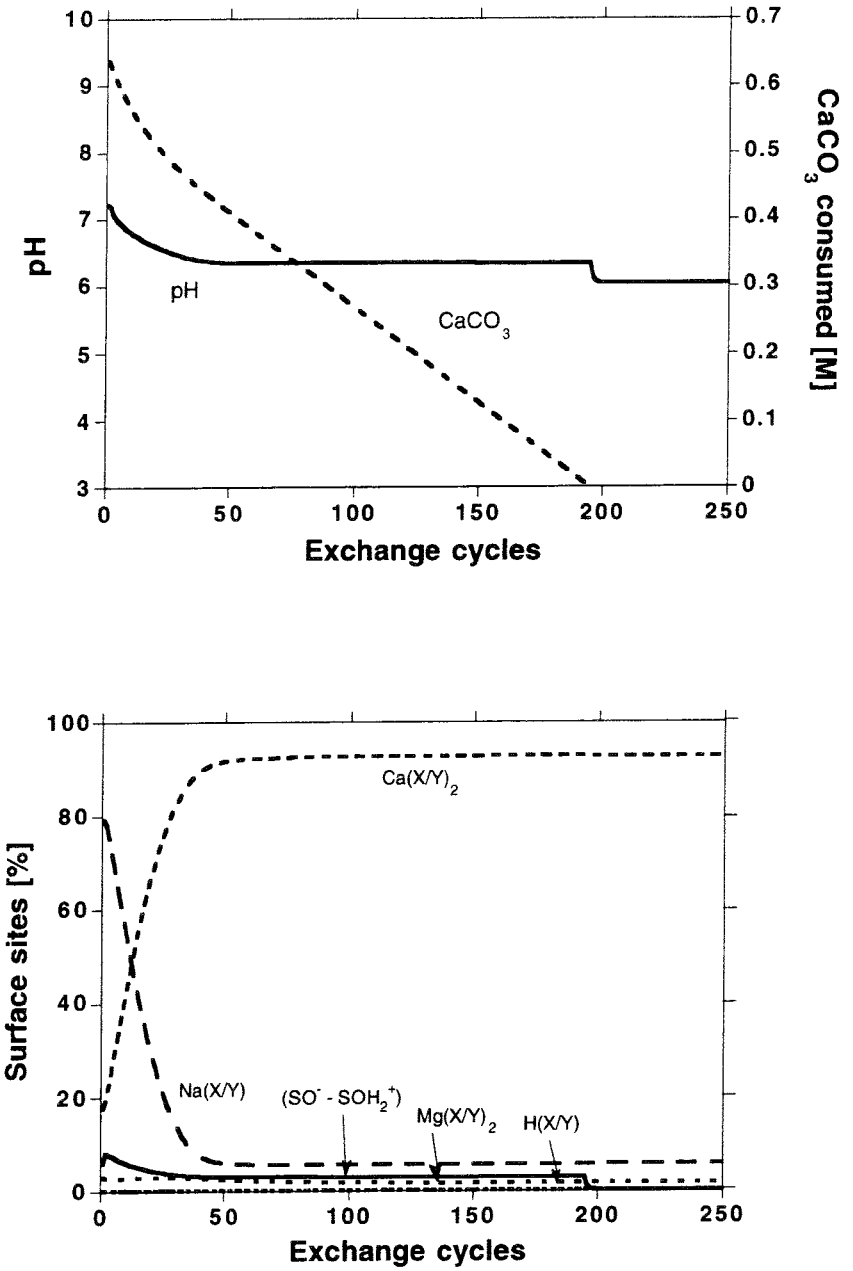

Figure 18 Bentonite in contact with Äspö groundwater. Prediction of pH, consumed calcite, exchangeable ions (Na^+, Ca^{2+}, Mg^{2+}, H^+) and negatively charged edge sites (SO^- - SOH_2^+) as a function of exchange cycles according to the mixing tank model. Two types of layer sites, X and Y, are considered in the model computations (see text). The composition of Äspö groundwater is given in Table 9. The surface chemical reactions are listed in Table 7.

Table 10: Predicted porewater composition of compacted bentonite in contact with Allard groundwater on the basis of the mixing tank model. Concentrations are given in mol/dm^3 [M], alkalinity (Alk) in eq/dm^3 and Na(X/Y) and $Ca(X/Y)_2$ as percentage distribution of the CEC (= X + Y layer sites). The CEC corresponds to 3.9 eq/dm^3.

cycle	pH	Na(X/Y)	$Ca(X/Y)_2$	Na^+	Ca^{2+}	$CaCO_3$	SO^--SOH_2^+	Alk	I
		[%]	[%]	[M]	[M]	[M]	[M]	[eq/dm^3]	[M]
1	7.36	78	18	1.7E-1	8.0E-3	6.4E-1	4.3E-3	3.7E-3	9.3E-3
2	8.37	78	18	2.3E-2	6.2E-5	6.3E-1	9.0E-3	1.9E-2	1.8E-2
10	8.38	73	23	2.1E-2	6.6E-5	5.6E-1	8.5E-3	1.7E-2	1.6E-2
50	8.19	58	38	1.7E-2	1.1E-4	2.6E-1	6.9E-3	1.6E-2	1.4E-2
90	8.04	42	52	1.5E-2	1.7E-4	5.5E-3	5.8E-3	1.5E-2	1.2E-2
150	6.91	40	54	4.3E-3	1.5E-5	0	9.0E-4	1.4E-3	3.8E-3
250	6.70	36	56	3.8E-3	1.5E-5	0	8.0E-4	1.3E-3	3.5E-3

Table 11: Predicted porewater composition of compacted bentonite in contact with Äspö groundwater on the basis of the mixing tank model. Concentrations are given in mol/dm^3 [M], alkalinity (Alk) in eq/dm^3 and Na(X/Y) and $Ca(X/Y)_2$ as percentage distribution of the CEC (= X + Y layer sites). The CEC corresponds to 3.9 eq/dm^3.

cycle	pH	Na(X/Y)	$Ca(X/Y)_2$	Na^+	Ca^{2+}	$CaCO_3$	SO^--SOH_2^+	Alk	I
		[%]	[%]	[M]	[M]	[M]	[M]	[eq/dm^3]	[M]
1	7.21	80	18	2.3E-1	9.2E-3	6.4E-1	8.2E-3	4.4E-3	1.6E-1
2	7.17	78	19	1.8E-1	2.8E-3	6.3E-1	1.0E-2	2.0E-2	2.0E-1
10	6.80	55	43	2.5E-1	1.1E-2	5.7E-1	8.4E-3	1.8E-2	2.8E-1
100	6.35	6	92	1.3E-1	1.1E-2	2.7E-1	4.6E-3	1.6E-2	4.6E-1
150	6.35	6	92	1.3E-1	1.1E-2	1.3E-1	4.6E-3	1.4E-2	4.6E-1
194	6.35	6	92	1.3E-1	1.1E-2	2.2E-3	4.6E-3	1.4E-2	4.6E-1
250	6.04	6	92	1.3E-1	1.1E-2	0	4.6E-3	6.0E-5	4.5E-1

6 Summary and Conclusions

The determination of the acid/base characteristics of surface functional groups and of ion exchange processes occurring at the solid/solution interface are essential to understanding and predicting surface-chemical reactions on montmorillonite. Two main types of surface sites are exposed at the surface of montmorillonite: structural-charge and variable-charge surface functional groups. Structural-charge sites located at the basal siloxane layer (layer sites) are accessible for ion exchange reactions. Edge OH groups, however, reveal an entirely different acid/base behaviour and are subject to ionisation reactions. Alkalimetric and acidimetric titrations of a purified Wyoming MX-80 bentonite were conducted in background media of three different ionic strengths (I = 0.005, 0.05 and 0.5 M) in order to establish the acid/base characteristics of edge sites.

Prior to the experimental studies, Wyoming bentonite MX-80 was pretreated using a well-established pretreatment procedure. The end product of the pretreatment procedure was characterised by XRD as Na-montmorillonite with small amounts of quartz and cristobalite as impurities. No calcite was found in the sample after completion of the pretreatment procedure. The CEC of Na-montmorillonite was determined to 108 meq/100 g for pretreated bentonite and to 85 meq/100 g for the bulk material. The BET surface area was (31.53 ± 0.16) m^2/g.

Potentiometric titrations of montmorillonite suspensions at ionic strengths I = 0.005 M, 0.05 M and 0.5 M were conducted as batch-type experiments. The reproducibility of the titration experiments indicates the absence of interfering side reactions such as the deprotonation of HCO_3^- dissolved in solution or the dissolution of the montmorillonite structure. Potentiometric titration hence is a suitable method for measuring the ionisation of OH groups exposed at the montmorillonite surface. Special attention has been paid to carefully calibrating the electrode system.

The results show that deprotonation of edge sites increases with increasing pH and ionic strength in the alkaline pH range. A net negative charge is developed on the edge surface in the pH range 6 to 10. Maximum deprotonation of edge sites is reached at pH ≈ 10. No apparent effect on surface reactions is observed when the $NaNO_3$ medium is replaced by a NaCl background electrolyte. Low surface proton densities are observed in the near-neutral pH range close to the expected point of zero net proton charge (PZNPC) of the edge sites, i.e., pH 6 - 7. The proton density on the surface of montmorillonite increases with decreasing pH in the acidic pH range. In this pH range, two simultaneously occurring surface reactions, i.e., protonation of edge OH groups

and ion exchange of the major cations for H^+ at layer sites, account for the observed overall proton density on montmorillonite.

The experimental results are interpreted in terms of a surface chemical model for montmorillonite with structural-charge surface sites, denoted as X layer sites, and variable-charge surface sites, denoted as edge OH groups, as the reactive surface functionalities. The interaction of protons with layer sites is due to ion exchange processes. Protolysis reactions occurring at OH groups are modelled using the configuration of the diffuse double-layer model (DDLM). The parameters of the two-site model, i.e., the total concentration of surface sites, the intrinsic acidity constants and the Na^+-H^+ exchange constant, are derived from the experimental data determined at I = 0.05 M using the fit programme FITEQL. The total concentrations of the surface sites are evaluated as TOT-OH = 2.84×10^{-5} mol/g and TOT-X = 2.2×10^{-5} mol/g, respectively. The intrinsic acidity constants of the OH groups are determined to pK_{a1}^{int} = (5.4 ± 0.1) and pK_{a2}^{int} = (6.7 ± 0.1), respectively. The thermodynamic constant of the Na^+-H^+ exchange at structural-charge sites is fitted to $\log K_X^\circ$ = (4.6 ± 0.1).

Experimental data of the potentiometric titrations of montmorillonite published in the open literature can be interpreted by implementing a third type of surface sites, denoted as Y layer sites, in the proposed two-site model for montmorillonite. The three-site surface chemical model comprises edge OH groups and two types of layer sites, i.e., X and Y layer sites. The Na^+-H^+ exchange constant for Y layer sites is estimated to $\log K_X^\circ$ = 3.0.

The near field chemistry under repository conditions is predicted with the aid of the proposed bentonite model. The model takes into account the presence of soluble impurities in bentonite (NaCl and $CaSO_4$) as well as ion exchange and protolysis reactions occurring at the surface of montmorillonite. Carbonate and silica concentrations are assumed to be controlled by calcite and quartz solubility.

The dependence of the chemical composition of Allard groundwater in contact with bentonite is modelled for increasing degrees of bentonite compaction. The model computations show that both the protolysis of edge OH groups of montmorillonite and calcite dissolution exert a strong control on the buffer capacity. Based on the proposed bentonite model a pH value of 7.3 and an alkalinity of 1.92×10^{-2} eq/dm^3 is predicted for the porewater of highly compacted bentonite.

Model predictions of the chemical composition of the porewater in moderately compacted bentonite (1.4 g/cm^3) are compared with experimental data documented by

Wanner et al. (1992). Theoretical and experimental data are consistent. The deviation of the predicted pH value of 8.4 from the measured ones of 9.0 and 9.2, respectively, may be due to uncertainties in the inventory and dissolution pathways of the soluble impurities.

The evolution of the chemical processes of highly compacted Na-bentonite with time is predicted under the assumption that the near field behaves like a mixing tank. Model computations are based on CEC = 85 meq/100g. Hence it is assumed that the number of surface sites accessible for protolysis and ion exchange reactions is given by the bentonite/water ratio regardless of the degree of bentonite compaction. In the modelling concept, bentonite porewater is completely exchanged by fresh groundwater during one water exchange cycle. Model computations are performed for up to 250 exchange cycles. The results of the calculations reveal a strong control of calcite dissolution and the acid/base properties of edge OH groups on pH and alkalinity in the near field. For Allard groundwater in contact with compacted bentonite, the pH in the near field is fixed around pH = 8.4 while calcite is present in the bentonite. It drops to about pH = 7.1 after complete removal of calcite from the backfill material, and, hereafter, slowly decreases with time to about pH = 6.8. The drop in pH is reflected in a decrease in the alkalinity. For Äspö groundwater in contact with compacted bentonite, lower pH values are predicted. The initial pH of about pH = 7.2 drops to about pH = 6 after exhaustion of calcite in bentonite. The drop in pH is accompanied by a drop in the alkalinity. Furthermore, a progressive change of Na-bentonite to Ca-bentonite is predicted for both groundwaters. The transformation rate depends on the amount of calcite present in bentonite and the chemical composition of the groundwater. Once the carbonate pool is depleted, the conversion of Na-bentonite to Ca-bentonite proceeds at a much lower rate.

In a previous, preliminary bentonite model (Wanner et al., 1992) the pH buffering effect of unaltered bentonite was determined by the calcite pool and its equilibrium reaction with the porewater. Under certain conditions, this reaction determined the pH, especially above pH values of about 9. The predicitions using the model of Wanner et al. (1992) agreed very well with the experimental determinations. However, the pH buffering effects below pH 9 could not be predicted with that model. The model developed in the present report includes all the relevant pH buffering effects over a wide range of the pH scale. The significance of soluble impurities is high as they lead to second and third order effects in the pH.

The bentonite model proposed in the present study has been developed based on experimental studies performed in dilute montmorillonite suspensions. Therefore the model may adequately predict solution compositions at low bentonite/water ratios.

However, care should be taken when extrapolations to higher degrees of bentonite compaction are envisaged. The critical constraints are: the effect of bentonite compaction on the number of available surface sites, i.e., CEC and the total number of edge sites, and on the dissolution of impurities. A validation of the proposed bentonite model combined with a sensitivity analysis should address these constraints. For a successful validation, however, more experimental data for compacted bentonite/water systems are required.

7 Acknowledgments

Gratitude is expressed to Stellan Holgersson for carrying out the titration experiments. We wish to thank Prof. Laurent Charlet (Université Joseph Fourier, Grenoble, France) for helpful discussions and thougthful comments on the manuscript.

8 References

Anderson, S.J. and Sposito G. (1991). Cesium-adsorption method for measuring accessible structural surface charge. Soil. Sci. Soc. Am. J. **55**, 1569 - 1576.

Avena, M.J., Cabrol, R. and de Pauli, C.P. (1990). Study of some physicochemical properties of pillared montmorillonites: acid-base potentiometric titrations and electrophoretic measurements. Clays Clay Min. **38**, 356 - 362.

Baes, C.F. and Mesmer, R.E. (1976). The hydrolysis of cations. Wiley Interscience, New York.

Berner, U. (1993). MIN_SURF. PSI version of MINEQL code, Würenlingen (personal communication).

Charlet, L., Schindler, P.W., Spadini, L., Furrer, G. and Zysset, M. (1993). Cation adsorptoin on oxides and clays: The aluminum case. Aquatic Science **55**, 291 - 303.

Davis, J.A. and Kent, D.B. (1990). Surface complexation modelling in aqueous geochemistry in: M.F. Hochella Jr. and A.F. White, Eds., Mineral-Water Interface Geochemistry, Mineralogical Society of America, 177 - 260.

Dzombak, D.A. and Morel, F.M.M. (1990). Surface complexation modelling: hydrous ferric oxides. John Wiley & Sons, New York.

Fletcher, P. and Sposito, G. (1989). The chemical modelling of clay/electrolyte interactions for montmorillonite. Clay Minerals **24**, 375 - 391.

Gallez, A., Juo, A.S.R. and Herbillon, A.J. (1976). Surface charge characteristics of selected soils in the tropics. Soil. Sci. Soc. Am. J. **40**, 601 - 608.

Huang, C.P. and Stumm, W. (1973). Specific adsorption of cations on hydreous α-Al_2O_3. J. Coll. Int. Sci. **22**, 231 - 259.

Hunter, R.J. (1981). Zeta potential in colloid science. Academic Press, London.

James, R.O. and Parks, G.A. (1982). Characterisation of aqueous colloids by their electrical double-layer and intrinsic surface chemical properties. Surf. Coll. Sci. **12**, 119 - 216.

Kruse, K. (1992). Die Adsorption von Schwermetallen an verschiedene Tone. Diss. ETH Nr. 9737.

Ludwig, Ch. (1992). GRFIT - a program for solving speciation problems. University of Berne, Berne, Switzerland (personal communication).

Madrid, L.E., Diaz, E., Cabrera, F. and Arambarri, P. (1983). Use of the three-plane model to describe charge properties of some ioron oxices and soil clays. J. Soil. Sci. **34**, 57 - 67.

Madrid, L.E., Diaz, E., and Cabrera, F. (1984). Charge properties of mixtures of minerals with variable and constant surface charge. J. Soil. Sci. **35**, 373 - 380.

Madrid, L.E and Diaz-Barrientos, E. (1988). Description of titration curves of mixed materials with variable and permanent surface charge by a mathematical model. 1. Theory. 2. Application to mixtures of lepidocrite and montmorillonite. J. Soil. Sci. **39**, 215 - 225.

Marshall, C.E. and Krinbill, C.A. (1942). The clays as colloidal electrolytes. J. Phys. Chem. **46**, 1077 - 1084.

McKinley, I.G. (1984). The geochemistry of the near field, Nagra NTB 84-48, Baden, Switzerland.

Morel, F.M.M. (1983). Principles of aquatic chemistry, John Wiley & Sons, New York.

Müller-Vonmoos, M. and Kahr, G. (1985). Langzeitverhalten von Bentonit unter Endlagerbedingungen. Nagra NTB 85-25, Baden, Switzerland.

Project Gewähr (1985). Nuclear Waste Managment in Switzerland: Feasibility studies and safety analyses, Nagra NGB 85-09, Baden, Switzerland.

Pulfer, K., Schindler, P.W., Westall, J.C. and Grauer, R. (1984). Kinetics and mechnaisms of dissolution of bayerite (γ-$Al(OH)_3$) in HNO_3-HF solutions at 298.2 K. J. Coll. Int. Sci. **101**, 554 - 564.

Sposito, G., Holtzclaw, K.M., Johnston, C.T. and LeVesque, C.S. (1981). Thermodynamics of sodium-copper exchange on Wyoming bentonite at 298 K. Soil. Sci. Soc. Am. J. **43**, 47 - 51.

Schindler, P. (1984). Surface complexation in: H. Sigel, Ed., Metal ions in biological systems. Vol. 18. M. Dekker, New York.

Sposito, G., Holtzclaw, K.M., Charlet, L., Jouany, C. and Page, A.L. (1983a). Sodium-calcium and sodium-magnesium exchange on Wyoming bentonite in perchlorate and chloride background ionic media. Soil. Sci. Soc. Am. J. **47**, 51 - 56.

Sposito, G., Holtzclaw, K.M., Jouany, C. and Charlet, L. (1983b). Cation selectivity in sodium-calcium, sodium-magnesium exchange, and calcium-magnesium exchange on Wyoming bentonite at 298 K. Soil. Sci. Soc. Am. J. **47**, 917 - 921.

Sposito, G. (1984). The surface chemistry of soils. Oxford University Press, New York.

Stadler, M. and Schindler, P.W. (1993). Modelling of H^{+}- and Cu^{2+}- adsorption on calcium-montmorillonite. Clays Clay Minerals **41**, 288 - 296.

Stumm, W., Huang, C.P. and Jenkins S.R. (1970). Specific chemical interactions athe stability of dispersed systems, Croat. Chim. Acta **42**, 223 - 245.

Stumm, W., and Morgan J.J. (1981). Aquatic chemistry. John Wiley & Sons, New York.

Van Olphen, H. and Fripiat, J.J. (1979). Data handbook for clay minerals and other non-metallic minerals. Pergamon Press. New York, 346pp.

Wanner, H. (1985). Modelling radionuclide speciation and solubility limits in the near-field of a deep repository. Mat. Res. Soc. Symp. Proc. **50**, 509 - 516.

Wanner, H. (1986). Modelling interaction of deep groundwaters with bentonite and radionuclide speciation. Nagra NTB 86-21, Baden, Switzerland.

Wanner, H., Wersin, P. and Sierro, N. (1992). Thermodynamic modelling of bentonite-ground water interaction and implications for near field chemistry in a repository for spent fuel. SKB TR 92-37.

Wanner, H., Albinsson, Y., Karnland, O., Wieland, E., Wersin, P. and Charlet, L. (1992). The bentonite chemical model: Phases II/III - surface characteristics of montmorillonite, MBT Progress Report, July 1993..

Werme, L. (1994). Personal communication.

Westall, J.C., Zachary, J.L. and Morel, F.M.M. (1976). MINEQL: A computer program for the calculation of chemical equlibrium composition in aqueous systems. Tech. Note, Dept. Civil Eng., Mass. Inst. Tech., Cambridge, MA.

Westall, J.C. (1982). FITEQL: A program for determination of chemical equilibrium constants from experimental data, Version 2.0, Report 82-02, Dept. of Chemistry, Oregon State Univ., Corvallis, OR.

Wieland, E., Wehrli, B and Stumm, W. (1988). The coordination chemistry of weathering: III. A generalization on the dissolution rates of minerals. Geochim. Cosmochim. Acta **52**, 1969 - 1981.

Wieland, E. and Stumm, W. (1992). Dissolution kinetics of kaolinite in acidic aqueous solutions at 25°C. Geochim. Cosmochim. Acta **56**, 3339 - 3355.

Wieland, E., Kohler, M. and Leckie, J.O. (1993). Adsorption of neptunium (Np(V)) onto mineral surfaces: Modelling surface complexation. Geochim. Cosmochim. Acta (accepted for publication)

Zysset, M. (1992). Die protoneninduzierte Auflösung von K-montmorillonite, Dissertation, Universität Bern.

List of SKB reports

Annual Reports

1977-78
TR 121
KBS Technical Reports 1 – 120
Summaries
Stockholm, May 1979

1979
TR 79-28
The KBS Annual Report 1979
KBS Technical Reports 79-01 – 79-27
Summaries
Stockholm, March 1980

1980
TR 80-26
The KBS Annual Report 1980
KBS Technical Reports 80-01 – 80-25
Summaries
Stockholm, March 1981

1981
TR 81-17
The KBS Annual Report 1981
KBS Technical Reports 81-01 – 81-16
Summaries
Stockholm, April 1982

1982
TR 82-28
The KBS Annual Report 1982
KBS Technical Reports 82-01 – 82-27
Summaries
Stockholm, July 1983

1983
TR 83-77
The KBS Annual Report 1983
KBS Technical Reports 83-01 – 83-76
Summaries
Stockholm, June 1984

1984
TR 85-01
Annual Research and Development Report 1984
Including Summaries of Technical Reports Issued during 1984. (Technical Reports 84-01 – 84-19)
Stockholm, June 1985

1985
TR 85-20
Annual Research and Development Report 1985
Including Summaries of Technical Reports Issued during 1985. (Technical Reports 85-01 – 85-19)
Stockholm, May 1986

1986
TR 86-31
SKB Annual Report 1986
Including Summaries of Technical Reports Issued during 1986
Stockholm, May 1987

1987
TR 87-33
SKB Annual Report 1987
Including Summaries of Technical Reports Issued during 1987
Stockholm, May 1988

1988
TR 88-32
SKB Annual Report 1988
Including Summaries of Technical Reports Issued during 1988
Stockholm, May 1989

1989
TR 89-40
SKB Annual Report 1989
Including Summaries of Technical Reports Issued during 1989
Stockholm, May 1990

1990
TR 90-46
SKB Annual Report 1990
Including Summaries of Technical Reports Issued during 1990
Stockholm, May 1991

1991
TR 91-64
SKB Annual Report 1991
Including Summaries of Technical Reports Issued during 1991
Stockholm, April 1992

1992
TR 92-46
SKB Annual Report 1992
Including Summaries of Technical Reports Issued during 1992
Stockholm, May 1993

1993
TR 93-34
SKB Annual Report 1993
Including Summaries of Technical Reports Issued during 1993
Stockholm, May 1994

Technical Reports
List of SKB Technical Reports 1994

TR 94-01
Anaerobic oxidation of carbon steel in granitic groundwaters: A review of the relevant literature
N Platts, D J Blackwood, C C Naish
AEA Technology, UK
February 1994

TR 94-02
Time evolution of dissolved oxygen and redox conditions in a HLW repository
Paul Wersin, Kastriot Spahiu, Jordi Bruno
MBT Technología Ambiental, Cerdanyola, Spain
February 1994

TR 94-03
Reassessment of seismic reflection data from the Finnsjön study site and prospectives for future surveys
Calin Cosma[1], Christopher Juhlin[2], Olle Olsson[3]
[1] Vibrometric Oy, Helsinki, Finland
[2] Section for Solid Earth Physics, Department of Geophysics, Uppsala University, Sweden
[3] Conterra AB, Uppsala, Sweden
February 1994

TR 94-04
Final report of the AECL/SKB Cigar Lake Analog Study
Jan Cramer (ed.)[1], John Smellie (ed.)[2]
[1] AECL, Canada
[2] Conterra AB, Uppsala, Sweden
May 1994

TR 94-05
Tectonic regimes in the Baltic Shield during the last 1200 Ma - A review
Sven Åke Larsson[1,2], Eva-Lena Tullborg[2]
[1] Department of Geology, Chalmers University of Technology/Göteborg University
[2] Terralogica AB
November 1993

TR 94-06
First workshop on design and construction of deep repositories - Theme: Excavation through water-conducting major fracture zones Såstaholm Sweden, March 30-31 1993
Göran Bäckblom (ed.), Christer Svemar (ed.)
Swedish Nuclear Fuel & Waste Management Co, SKB
January 1994

TR 94-07
INTRAVAL Working Group 2 summary report on Phase 2 analysis of the Finnsjön test case
Peter Andersson (ed.)[1], Anders Winberg (ed.)[2]
[1] GEOSIGMA, Uppsala, Sweden
[2] Conterra, Göteborg, Sweden
January 1994

TR 94-08
The structure of conceptual models with application to the Äspö HRL Project
Olle Olsson[1], Göran Bäckblom[2], Gunnar Gustafson[3], Ingvar Rhén[4], Roy Stanfors[5], Peter Wikberg[2]
1 Conterra AB
2 SKB
3 CTH
4 VBB/VIAK
5 RS Consulting
May 1994

TR 94-09
Tectonic framework of the Hanö Bay area, southern Baltic Sea
Kjell O Wannäs, Tom Flodén
Institutionen för geologi och geokemi, Stockholms universitet
June 1994

TR 94-10
Project Caesium–An ion exchange model for the prediction of distribution coefficients of caesium in bentonite
Hans Wanner[1], Yngve Albinsson[2], Erich Wieland[1]
[1] MBT Umwelttechnik AG, Zürich, Switzerland
[2] Chalmers University of Technology, Gothenburg, Sweden
June 1994

TR 94-11
Äspö Hard Rock Laboratory Annual Report 1993
SKB
June 1994

TR 94-12
Research on corrosion aspects of the Advanced Cold Process Canister
D J Blackwood, A R Hoch, C C Naish, A Rance, S M Sharland
AEA Technology, Harwell Laboratory, Didcot, Oxfordshire, UK
January 1994

TR 94-13
Assessment study of the stresses induced by corrosion in the Advanced Cold Process Canister
A R Hoch, S M Sharland
Chemical Studies Department, Radwaste Disposal Division, AEA Decommissioning and Radwaste, Harwell Laboratory, UK
October 1993

TR 94-14
Performance of the SKB Copper/Steel Canister
Hans Widén[1], Patrik Sellin[2]
[1] Kemakta Konsult AB, Stockholm, Sweden
[2] Svensk Kärnbränslehantering AB, Stockholm, Sweden
September 1994

TR 94-15
Modelling of nitric acid production in the Advanced Cold Process Canister due to irradiation of moist air
J Henshaw
AEA Technology, Decommissioning & Waste Management/Reactor Services, Harwell, UK
January 1994

TR 94-16
Kinetic and thermodynamic studies of uranium minerals. Assessment of the long-term evolution of spent nuclear fuel
Ignasi Casas[1], Jordi Bruno[1], Esther Cera[1], Robert J Finch[2], Rodney C Ewing[2]
[1] MBT Tecnología Ambiental, Cerdanyola, Spain
[2] Department of Earth and Planetary Sciences, University of New Mexico, Albuquerque, NM, USA
October 1994

TR 94-17
Summary report of the experiences from TVO's site investigations
Antti Öhberg[1], Pauli Saksa[2], Henry Ahokas[2], Paula Ruotsalainen[2], Margit Snellman[3]
[1] Saanio & Riekkola Consulting Engineers, Helsinki, Finland
[2] Fintact Ky, Helsinki, Finland
[3] Imatran Voima Oy, Helsinki, Finland
May 1994

TR 94-18
AECL strategy for surface-based investigations of potential disposal sites and the development of a geosphere model for a site
S H Whitaker, A Brown, C C Davison, M Gascoyne, G S Lodha, D R Stevenson, G A Thorne, D Tomsons
AECL Research, Whiteshell Laboratories, Pinawa, Manitoba, Canada
May 1994

TR 94-19
Deep drilling KLX 02. Drilling and documentation of a 1700 m deep borehole at Laxemar, Sweden
O Andersson
VBB VIAK AB, Malmö
August 1994

TR 94-20
Technology and costs for decommissioning the Swedish nuclear power plants
Swedish Nuclear Fuel and Waste Management Co, Stockholm, Sweden
June 1994

TR 94-21
Verification of HYDRASTAR: Analysis of hydraulic conductivity fields and dispersion
S T Morris, K A Cliffe
AEA Technology, Harwell, Didcot, Oxon, UK
October 1994

TR 94-22
Evaluation of stationary and non-stationary geostatistical models for inferring hydraulic conductivity values at Äspö
Paul R La Pointe
Golder Associates Inc., Seattle, WA, USA
November 1994

TR 94-23
PLAN 94
Costs for management of the radioactive waste from nuclear power production
Swedish Nuclear Fuel and Waste Management Co
June 1994

TR 94-24
Äspö Hard Rock Laboratory
Feasibility and usefulness of site investigation methods. Experiences from the pre-investigation phase
Karl-Erik Almén (ed.)[1], Pär Olsson[2], Ingvar Rhén[3], Roy Stanfors[4], Peter Wikberg[5]
[1] KEA GEO-Konsult
[2] SKANSKA
[3] VBB/VIAK
[4] RS Consulting
[5] SKB
August 1994

TR 94-25

Kinetic modelling of bentonite canister interaction. Long-term predictions of copper canister corrosion under oxic and anoxic conditions

Paul Wersin, Kastriot Spahiu, Jordi Bruno
MBT Tecnología Ambiental, Cerdanyola, Spain

September 1994